Incision rate of the Yellow River in Northeastern Tibet constrained by 10Be and 26Al cosmogenic isotope dating of fluvial terraces: implications for catchment evolution and plateau building

Aude Perrineau, Jerome van Der Woerd, Yves Gaudemer, Jing Liu-Zeng, Raphaël Pik, Paul Tapponnier, Robert Thuizat, Ronzhang Zheng

Incision rate of the Yellow River in northeastern Tibet constrained by ^{10}Be and ^{26}Al cosmogenic isotopes dating of fluvial terraces : implications for catchment evolution and plateau building

A. Perrineau (1,2) J. van der Woerd (2), Y. Gaudemer (1), Jing Liu-Zeng (3), R. Pik (4), P. Tapponnier (1), R. Thuizat (2), Zheng Rongzhang(5)

1. Laboratoire de Tectonique, Institut de Physique du Globe de Paris - UMR 7154, 4 place Jussieu, 75254 cedex 05, Paris, France
2. Institut de Physique du Globe de Strasbourg – UMR CNRS/UDS 7516, École et Observatoire des Sciences de la Terre, University of Strasbourg, 5 rue René Descartes, 67084 Strasbourg cedex, France
3. Institute of Tibetan Plateau Research, Chinese Academy of Sciences, 18 Shuang Qing Rd., PO Box 2871, Beijing 100085, China
4. Centre de Recherche Pétrographiques et Géochimiques - UPR1167, 15 rue Notre-Dame des Pauvres, 54501Vandoeuvre-lès-Nancy, France
5. China Earthquake Administration, Beijing, China.

Accepted for publication in Geological Society of London special paper.

Number of words of text: 12087
Number of references: 79
Number of tables: 2
Number of figures: 17

Abbreviated title: Incision rate of the Yellow River in northeastern Tibet

Keywords : 10Be, 26Al, cosmogenic nuclide dating, river incision, Yellow River, northeastern Tibet

Abstract

Unlike other large rivers flowing out of Tibet the Yellow River escapes from the plateau towards the northeast crossing no less than 5 NW-SE striking, actively growing mountain ranges and intervening basins. Thick Plio-Quaternary deposits and high fluvial terraces testify to a phase of aggradation and sediment infill up to the average surface elevation (3200-3250 m a.s.l.) of the Gonghe, Guide and Qinghai Lake basins. A set of 7 main terraces across the Gonghe Basin suggest progressive downcutting of the Yellow River carving the present 500 m-deep Longyang gorge at the basin exit. ^{10}Be and ^{26}Al concentrations in quartz of surface and sub-surface samples of four terraces constrain the timing of incision of the Yellow River by determining the burial age of the deposit and the exposure age of its surface. Modeling of the depth dependence of the ^{10}Be concentration and of the ^{26}Al/^{10}Be ratio allows constrain the onset of the ongoing phase of incision to 120-250 ka. These ages suggest long-term incision rates between 2 and 6 mm/year. Together with the present morphology of the Yellow River terraces across the Gonghe basin and the Longyang gorge the ages imply rapid river catchment evolution and interaction between river dynamics, tectonic and climate in the northeastern edge of the Tibetan plateau.

1) Introduction

How and when the Tibetan plateau reached its present altitude and shape are important to investigate as the topography influences atmospheric circulations, thus the climate, but also because it may be used to constrain models of Tibetan plateau evolution (e.g., Tapponnier *et al.,* 1982; Peltzer & Tapponnier, 1988; England & Houseman, 1986; Houseman & England, 1993; Royden *et al.,* 1997; Fluteau *et al.,* 1999; Tapponnier *et al.,* 2001; Liu-Zeng *et al.,* 2008). In the stepped growth model of Tibet of Tapponnier *et al*. (2001), northeastern Tibet is the youngest part of the plateau that formed from Pliocene time to present (Meyer et *al*., 1998; Métivier *et al.,* 1998). The region is characterized by narrow actively growing ranges (e.g., Tapponnier *et al.,* 1990; Meyer *et al.,* 1998; Van der Woerd *et al.,* 2001) that separate flat rapidly filling closed sedimentary basins (Meyer *et al*., 1998, Métivier *et al.,* 1998; Van der Woerd, 1998). Such process may have been active in the central part of the Tibetan plateau, leading to the formation of a high topography at about 5000 m a.s.l.. From this point of view, the northeastern Tibetan region is a key place to unravel processes of the formation of the Tibetan Plateau. Understanding the different roles of tectonics, climate and the evolving drainage is thus important to constrain the formation of the present topography of Tibet (e.g., Clark *et al*., 2004; Liu-Zeng *et al.,* 2008).

The Yellow River, together with the Jinsha, Lancang (Mekong), and Nu (Salween) rivers, drains the Tibetan plateau on its eastern rim (Figure 1). While its source is located on the high summer monsoon influenced central plateau, like the other large rivers, it does not escape the plateau to the southeast but is captured to the north after a hairpin loop in the Zoige (Roergai) basin (Figure 1; e.g., Harkins *et al.,* 2007). As it flows back to the northwest, north of the Anyemaqen Shan, it enters regions of lesser precipitation that barely feed the river. This particularity makes the river sensitive to any north-south shift of the northern monsoon limit,

which depends on climate variations (e.g., Benn & Owen, 1998; Joussaume, 1999). Both the fact that the river crosses a relatively dry northeastern Tibet allowing long-term preservation of the terraces and its high sensitivity to climate change probably in part explains the long sequence of fluvial terraces found all along the river from the Anyemaqen to the Ordos, in northern China.

The terraces of the Yellow River, near Gonghe (Figure 2) or near Lanzhou (e.g., Wang *et al*., 2010; Li, 1991), have been commonly interpreted both to testify the first occurrence of the Yellow River in northeast Tibet and as a record of regional plateau surface uplift (e.g., Li *et al*. 1997; Li, 1991; Harkins *et al*. 2007). In this study, we will show that the terraces instead more likely indicate rapid incision of the river after a phase of damming and deposition of the Yellow River. In fact, probably better than anywhere else in Tibet, the terraces of the Yellow River across the Gonghe basin illustrate a process of plateau building that involves damming of the drainage by active range growth and rapid filling of closed sedimentary basins (e.g., Métivier *et al*., 1998; Meyer *et al*., 1998).

In this paper, we describe the terraces of the Yellow River in the Gonghe basin. We present the ^{10}Be and ^{26}Al exposure ages obtained on four different terrace levels that allow to constrain both the incision history of the Yellow river across the Gonghe basin and the uplift rate of the surrounding ranges. We then discuss the implications on the basin history, and on the local and regional tectonics.

2) Geological and geomorphic setting

2.1 The Yellow River, basins and ranges

From the Zoige basin, east of Anyemaqen and south of the Kunlun fault to the Gobi platform, over a length of 500 km (or river length of >1000 km), the elevation drop of the Yellow River reaches about 2500 m as it crosses several sedimentary basins (Tongde, Gonghe, Guide, Xunhua, Linxia), all separated by actively growing ranges (Heka Shan, Waligong Shan, Kongma Shan, Laji Shan) (Figures 1-3). Along this stretch, the river crosses no less than 3 active strike-slip fault systems and about 6 active thrusts implying interactions of river dynamics and active tectonics. Across both the Kunlun and Haiyuan left-lateral strike-slip faults (Figure 1), the Yellow River is deflected 80-90 km left-laterally (e.g., Gaudemer *et al*., 1989, 1995; Van der Woerd *et al*., 2002). Right-lateral movement along the Haiyen fault that connects with the more easterly trending Riyue-Laji-Kongma Shan thrusts contribute to the range growth along the northeastern border of the Guide basin. The Tongde basin is bounded to the north by the southvergent Heka Shan (Figure 1; Harkins *et al*., 2007). The Gonghe basin is limited to the north and south by active thrusts. In the south, thrusts are northvergent in the west and southvergent in the east, and their activity is attested by the magnitude Mw 6.9 1990 seismic event (Chen *et al*., 1996). In the north, the Qinghainan Shan thrusts are southvergent to the west and are attested by folded and uplifted alluvial fans and terraces (Van der Woerd, 1998) and northvergent to the east (Waligong Shan). Intensely faulted and folded Neogene series in front of the Ryue-Laji Shan (Fang *et al*., 2005) together with detrital zircon ages and their provenance from the Laji Shan (Lease *et al*., 2007) imply major shortening phases during the Plio-Quaternary along the northern Guide basin. Additional but less important thrusting also occurs along the western Linxia basin (Fang *et al*., 2003; Zheng *et al*., 2003), across the Lanzhou thrusts (Wang *et al*., 2010) and across the Tianjing-Mibo Shan north of the Haiyuan fault (Gaudemer *et al*., 1995). Most of the elevation change of the Yellow River occurs between Zoige and Linxia and the steepest river gradients are found in the gorges across the Waligong and Kongma Shan (Figure 3).

At the northeastern exit of the Gonghe basin, the Yellow River crosses the Waligong mountains carving the 500 m-deep Longyang Gorge (Longyangxia in Chinese) (Figures 2 and 3). Since 1986, an artificial dam has been built at the entrance of the Longyang gorges forming the about 100 m deep Longyangxia Reservoir (water level at 2568 m in October 2004). The NW-SE trending Waligong Shan is composed of two massifs, the western and eastern Waligong, each one bounded to the east by active west- to southwest-dipping thrusts (Figure 2). The western Waligong thrust juxtaposes the Waligong granite on top of red sandstones of Late Miocene-Pliocene age (Pan, 1994; Qinghai Geological Bureau, 1988; Figure 4e), similarly to the thrust of the eastern Waligong at the Guide basin western margin.

The most striking evidence for ongoing uplift is the impressive Longyang gorges carved by the Yellow River as it crosses the Waligong range (Figures 4a and 4b). The slope of the Yellow River increases dramatically at the entrance of the Longyang gorges to about 0.5° (Figure 3). The height of the bedrock cliff reaches about 300-500 m in the gorge (Figure 4). Other evidences for active tectonic uplift are given by the abraded bedrock abandoned above the gorge. At present, the bedrock slopes towards the west as expected if it were back-tilted to the west due to uplift of the Waligong on top of a west dipping thrust (Figure 5).

2.2 The Yellow river terraces across the Gonghe Basin

The Gonghe Basin is a northwest-southeast trending 250 x 50 km-wide sedimentary basin (Figures 1 and 2). It is bounded to the north by the actively growing Qinghainan Shan and to the south by the Ngola Shan (or Gonghenan Shan) and the Heka Shan. It is filled with up to 1200 meters of Quaternary sediments (Qinghai Geological Bureau, 1988 ; Métivier *et al.*, 1998). Semi-arid climatic conditions prevail over most of the basin (annual precipitation

average 250-350 mm; Domroes & Peng, 1988) and sand dune fields occupy the eastern part of it (Figures 2 and 4c). The basin is almost entirely internally drained except in its eastern part where it is crossed by the Yellow River. In contrast with the Qinghai Lake basin located just north of the Qinghainan Shan (Figure 1) and occupied by the largest fresh water lake of China (4500 sq.m and about 27 m deep; Qin, 1992), only small lakes are visible across the Gonghe basin. Evidence for higher lake levels can be seen in abandoned lake shore lines or lake deposits (e.g. around Dalian lake or Chaka salt lake; Figure 6; van der Woerd, 1998). Despite their proximity, both basins have slightly different present climatic regimes characterized by dryer conditions in Gonghe (Domroes & Peng, 1988).

As it crosses the Gonghe basin and incises through the sediment pile (Figure 4d), the Yellow River has abandoned a set of terraces that form huge fan shaped stairs across the entire 50 km-width of the basin (Figure 2). The freshness of the terraced landscape (Figure 4c) together with the fact that regressive erosion from the Yellow River gorge itself has not yet captured the central drainage of the Gonghe basin indicate that the Yellow River incision occurred recently as suggested by several authors (e.g., Li, 1991; Métivier *et al*., 1998; Zhang *et al*. 2004; Van der Woerd, 1998). The large, up to 10 km-wide and 40-50 km long, terraces across the basin are mostly flat with slopes toward the north comparable to the present Yellow River slope (0.15-0.3°) in the same area (Figures 3a-3c). From the present river bed to the top we numbered the main and largest terrace levels T0 to T7 (Figures 2 and 3). We designate the highest and largest terrace T7 knowing that it also corresponds to the regional surface level of basins around 3200-3250 m a.s.l. (Figures 2 and 3). This surface can be easily recognized on satellite images or on digital elevation models (SRTM DEM) as it forms flat areas that merge smoothly with the piedmont bajadas of the surrounding ranges (Figures 2 and 7a). A similar surface level correlates with the top of the sediment fill in the Guide and Tongde basin

(Fothergill & Ma, 1999; Fang *et al*., 2005; Harkins *et al*., 2007). Interestingly, this level is also the highest paleo-lake stand of the Qinghai lake basin to the north (~ 3250 m, e.g., Lister *et al*., 1991; Rhode *et al*., 2007, 2010; Liu *et al*., 2010; Fang *et al*., 2005).

T7 is clearly recognized as a fluvial terrace deposit at the entrance of the Gonghe basin north of Heka Shan (Figures 2 and 7b). T7 is now covered by a 2 m-thick layer of eolian loess overlying a 15 cm-thick reddish paleosol (B-horizon; Figures 8a and 8b; Pan, 1994). The abandonment of T7 marks the onset of incision of the Yellow river in the Gonghe basin. The other major terrace levels (T6 to T1) are also composed of fluvial pebbles and gravels and are devoid or only covered by a thin loess cover across the Gonghe basin. Clear steep risers up to several tens of meters high separate the main terrace levels (Figures 2d and 4c). In several places, as can be clearly seen on satellite images (Figure 2), these risers disappear under wind-blown sand dune fields because of favorable accumulation at the north-south trending risers which are almost perpendicular to the main northwest blowing winds.

For a long time the Yellow River terraces have been recognized as geomorphic markers of the active tectonics of northeastern Tibet during the Quaternary (e.g., Li, 1991; Lu *et al*., 2004; Sun, 2005; Li *et al*., 1997). From Lanzhou to Gonghe, their Early Pleistocene to late Pleistocene ages (e.g., Li *et al*., 1997) have been interpreted to represent phases of regional plateau uplift. In contrast, Harkins *et al*. (2007) have recently proposed, from a geomorphological analysis of the upper Yellow River gorge and its tributaries between Tongde and Zoige basins that the Yellow river propagated upstream due to headward incision. From OSL and C-14 ages of low terraces 10 to 140 m above the present river bed in Tongde and upstream that range from 9 to 140 ka, (Figure 3), they infer an onset of incision from the top of the basin fill in Tongde at about 400-500 ka (Craddock *et al*., 2010). In more details,

their results imply the upward propagation of a wave of incision starting around 500 ka in Tongde with incision rates of about 2.5 mm/yr that slowed down as incision progressed to less than 1 mm/yr at present (Harkins *et al*., 2007; Figure 3).

The terraces in Gonghe have not been directly dated so far. Thermoluminescence (TL) dating of loess covering 7 terraces in Linxia give ages that range from 10 to 160 ka (Li *et al*., 1997) and due to the similar setting of terraces in Gonghe, the oldest of these ages has been attributed to the highest terrace in Gonghe (Li, 1991; Li *et al*., 1997; Zhang *et al*., 2004; Fothergill & Ma, 1999). However, from paleomagnetostratigraphic studies in Guide and Linxia, it has been argued that the highest terrace in Guide postdates closely the shallowest dated sediments at 1.8 Ma (Fang *et al*., 2005), and that the Yellow river started incising in Gonghe at about 1.1 Ma (Yan *et al*., 2004), in agreement with the inference of a post 500 ka incision of the Yellow River in Tongde and the upward propagation of a wave of incision (Harkins *et al*., 2007).

It is thus necessary to directly date the terraces, to determine their age of deposition and abandonment to constrain the incision history of the Yellow River and the rates of tectonic uplift of the narrow ranges cross-cut by the river.

3) Terrace dating, results and interpretation

3.1 Cosmogenic nuclide dating method

Cosmogenic nuclides are produced in situ by the interactions between secondary cosmic ray particles and surface rocks. Cosmogenic nuclides accumulate in rocks as long as they stay at/near to the surface of the Earth. ^{10}Be and ^{26}Al are mainly produced in quartz from O and Si by spallation and muonic capture, and the ubiquity of this mineral makes it a favoured target.

The concentration of cosmogenic radioactive nuclides in a rock, N, is given by:

$$\frac{dN}{dt} = P - \lambda N \tag{1}$$

where λ is the decay constant of the nuclide considered and P is the production rate, which depends on the geographic location and altitude. For sub-surface samples, the production rate decreases exponentially with depth following:

$$P(z) = P(0).\exp\left(-z\frac{\rho}{\Lambda}\right) \tag{2}$$

where $P(0)$ is the production rate at the surface, z the depth of the sample, ρ the density of the overlying material and Λ the attenuation length of the interacting particle. Analysing deep (shielded) samples may give access to the amount of inheritance. Indeed, samples situated below several times the penetration depth are shielded from cosmic radiations and their cosmogenic nuclide concentrations thus correspond to nuclides accumulated before being deposited, i.e., the inherited component. When inheritance and erosion are assumed to be negligible, then the minimum exposure age of a sample is given by:

$$t_{\min} = \frac{1}{\lambda}\ln\left(\frac{1-\lambda N}{P}\right). \tag{3}$$

Taking into account erosion, inheritance and production by muons, the number of ^{10}Be atoms grows with time according to:

$$N(z,\Delta t) = N_0(z,\Delta t)\exp(-\lambda\Delta t) + \left[\frac{P_n}{\lambda+\frac{\rho}{\Lambda_n}\varepsilon}\exp\left(-\frac{\rho}{\Lambda_n}z\right)+\right]\times\left(1-\exp\left(-(\lambda+\left(\frac{\rho}{\Lambda_n}\varepsilon\right)\Delta t\right)\right)+\left[\frac{P_m}{\lambda}\exp\left(-\frac{\rho}{\Lambda_m+\frac{\rho}{\Lambda_m}\varepsilon}z\right)\right]\times\left(1-\exp\left(-(\lambda+\left(\frac{\rho}{\Lambda_m}\varepsilon\right)\Delta t\right)\right)\right) \tag{4}$$

where $N_0(z,\Delta t)$ is the inherited component, (n,m) subscripts for spallation by neutron and muons, respectively.

Samples were processed in the Cosmogenic Nuclides Laboratory of the University of

Strasbourg following standard methods described in Kohl and Nishiizumi (1992). $^{10}Be/^{9}Be$ and $^{26}Al/^{27}Al$ ratios were determined by accelerator mass spectrometry (AMS) at the ASTER (CEREGE, Aix-en-Provence) facility except two samples (Qi4-29-1 and Qi4-29-19, Table 1), which were measured at the Center for Accelerator Mass Spectrometry at Lawrence Livermore National Laboratory (Table 1). Natural ^{9}Be has been assumed to be not present in our samples after a set of samples has been checked by ICP-MS. The total ^{9}Be concentration is thus determined by the amount of carrier added to the sample.

The ^{26}Al concentrations were measured in a subset of samples to better constrain the exposure history of the terraces. As the stable isotope ^{27}Al is naturally present in quartz minerals, sample content of natural ^{27}Al was measured by ICP-MS before addition of ^{27}Al carrier. ^{10}Be and ^{26}Al have different decay constants and production rates, but the same production profiles. They can thus be analysed together and compared. In case of a simple exposure history, without a period of burial, the $^{26}Al/^{10}Be$ nuclide ratio approximates 6.75 (Balco, 2009).

Nuclide concentrations were determined from the AMS measurements and the amount of corresponding stable isotope (Table 1). Ages were modelled using the CRONUS online calculator (Balco *et al.,* 2008) version 2.2 (April 2009). Sub-surface sample concentrations have been modelled by fitting the sample concentrations following equation (2) (see also, Granger & Smith, 2000) and using the constant surface production rate determined by the CRONUS calculator (see details below). We used the revised ^{10}Be decay constant of $5.1 \pm 0.26 \times 10^{-7}$ a^{-1} of Nishiizumi *et al*. (2007) and the ^{26}Al decay constant of 9.83×10^{-7} a^{-1}, following Balco *et al*. (2008). Penetration depths used for depth profiles ages calculation are 160 $g.cm^{-2}$ for neutrons and 1500 $g.cm^{-2}$ for muons (Gosse & Phillips, 2001; Granger & Smith, 2000). We used densities of 2.65 for quartz, 2.7 for granite, 2.5 for a mix

gravel/pebble/cobble deposit, 1.8 for soil, 1.4 for loess. No topographic shielding correction was needed given the extent and flatness of the terraces. All other data used in the calculator, as advised by Balco et *al*. (2008) and Frankel (2010), are given in Table 1.

The largest analytical uncertainty comes from the production rate estimation (Gosse & Phillips, 2001). Balco *et al*. (2008) estimated this uncertainty to approximate 10%. It is however larger for depth samples because uncertainties on penetration depths (6%), sample depth (0,5%) and density of overlying material (2-3%) must be added. Final uncertainties on production rates are then comprised between 10 and 12%. Uncertainties from the chemical processing are low (1-2%). Uncertainties from the AMS measurement are comprised between 1.8 and 3.5%. Total analytical uncertainties on ages, not considering modeling errors, thus range from 11% to 13% (Table 1).

We sampled four different terrace levels for cosmogenic dating, T7 and T5 in the basin, and two strath terrace levels in the gorge, WRB (Waligong right bank) and WLB (Waligong left bank) (Figure 2, Table 1).

3.2 Cosmogenic nuclide measurements

3.2.1 Terrace T7 samples

Stratigraphy

On the southern side of the Gonghe basin, north of Heka Shan and on the right bank of the Yellow River, clean exposure of the top 10 m of the T7 level can be seen in a gravel quarry used for road constructions (Figures 2c, 7 and 8). The terrace conglomerate is a thick fill deposit, composed of gravels, pebbles and cobbles with a few 5 to 50 cm-thick and several

meters long sand lenses (Figure 8c). It is covered by a 15 cm-thick reddish paleosol (Figure 8b), itself covered by about 2 m of eolian loess (in the following sections, layer and sample depths are given relative to present ground surface, i.e., the top of the loess deposit). The conglomerate pile is marked by an angular unconformity at around 3.5-4 m depth. In an EW section, the ~5° west dipping pebble layers and sand lenses are intersected by overlying horizontal layers. In the NS section, the angular unconformity disappears, but a clear layer transition can be seen in the section approximately at the same depth (Figure 8). The two conglomerate units will be called C1 and C2 from bottom to top in the following sections. The top 20 cm of the C2 conglomerate, just below the paleosol, is marked by a visible increase in the amount of whitish quartz-vein centimetric pebbles (Figure 9; Table 1). Our field observations and inspection of the quarry cliffs have not allowed to distinguish any other sedimentation interruption or other unconformities. Note that the latter would be difficult to detect since there is no obvious change in the nature and origin of the material deposited. Therefore, in the following discussion, we will consider the section analyzed as a sequence of two depositional events (assuming that other sedimentation interruptions, if present, lasted only for short periods compared to the whole life time of the terrace), followed by the formation of a paleosol, itself followed by the deposition of loess.

Sampling

From depths of 2 to 7.5 m we collected 16 quartz-rich samples for cosmogenic exposure dating along two nearby vertical profiles (Figure 8, Table 1). At a depth of 2 m, a cobble was found above the paleosol but below the loess cover (sample Qi4-29-1). Below the paleosol, in unit C2, we collected a large number of centimeter-sized quartz-vein pebbles at a depth of 2.10 ± 0.10 m. These pebbles were sorted by size and analyzed as 4 separated amalgamated samples (samples Qi4-29-27a, b, c and d; Table1; Figure 9). Four additional samples are

individual quartz-rich cobbles (quartz vein or granitoid) from 2.3 to 3.2 m. In unit C1, three sand lenses were sampled at 3.7, 3.9 and 7.5 m (samples Qi4-29-14, 15 and 23, respectively; Table 1). The 4 remaining samples are individual quartz-rich cobbles at 4.00, 4.80, 6.15 and 6.75 m (samples Qi4-29-16, 24, 21 and 22; Table 1). Among those 16 samples, 13 were analyzed for ^{26}Al (Table 1).

^{10}Be nuclide concentrations

^{10}Be concentrations range from 235000 to 1500000 at/g(qtz) for most of the samples, except 2 that have highest concentrations of about 2 millions at/g(qtz) (Figure 10a, Table 1). Lowest concentrations are those of cobble samples Qi4-29-21 and Qi4-29-11 with, 235000 and 405000 at/g(qtz), respectively. The sand lens samples have larger concentrations of 445000, 505000 and 785000 at/g(qtz). The large concentrations of 1500000 at/g(qtz) is reached for samples right below the soil-conglomerate interface, samples Qi4-27a, b,c and d (Table 1).The whole sequence of ^{10}Be concentrations measured in the different samples do not show a monotonous exponential decrease with depth but imply either sequential deposition (e.g., Shaller *et al*., 2002; Matmon *et al*., 2009) or a variable inheritance between samples (e.g., Anderson *et al*., 1996; Mériaux *et al*., 2004, 2005; LeDortz *et al*., 2009). In particular the different type of samples collected, individual cobbles, sand lenses or amalgamated pebbles may have various pre-exposure components (e.g., Oskin *et al*., 2008). However, within each unit, C1 and C2, the sample concentrations show an exponential decrease with depth linked to their respective exposure histories (Figure 10).

^{26}Al nuclide concentrations

The ^{26}Al concentrations were measured in 13 samples (Table 1). The concentrations range from 2 to 9 millions at/g(qtz) and imply ^{26}Al/^{10}Be ratios that vary between 4.12 to 6.06

(Figures 10 and 11; Table 1). Low $^{26}Al/^{10}Be$ ratio values usually result from differential decay of ^{10}Be and ^{26}Al caused by shielding from cosmic rays after a period of nuclide accumulation (Bierman, 1994). None of the samples have typical simple exposure surface $^{26}Al/^{10}Be$ ratio of 6.75 implying either shielding of the section or a significant component of inherited nuclides. Disregarding a few anomalous samples, such as, Qi4-29-1 that is probably a reworked cobble found above the paleosol, Qi4-29-9 and Qi4-29-22 that have high ^{10}Be concentrations (large inheritance) and the sand samples, the $^{26}Al/^{10}Be$ ratio decreases slightly from 6 to 5.7 between 2 m to 6.15 m depth (Figure 10b). The sand lenses have lower $^{26}Al/^{10}Be$ ratios of about 4.8 to 5.06, which may indicate incorporation of material with inherited low $^{26}Al/^{10}Be$ ratios. We note that this might also be the case of present river sands, which have a ratio of about 5.28 (sample Qi4-43A, Table 1). We will jointly model (see below) the ^{10}Be concentration profile and the $^{26}Al/^{10}Be$ ratio to constrain the age of deposition and abandonment of the T7 level.

3.2.2 Terrace T5 samples

Geomorphic setting

Terrace T5 is one of the largest terraces southwest of Gonghe situated about 150 m below T7 (Figures 2, 3, 12). It is flat in its northern part where the surface is characterized by a tight pebble and cobble pavement (Figure 12). At places, sand dunes (barkanes) travel southeastwards across the terrace with the probable consequence of incorporation of modern sand below the pavement and abandonment of sandy patches at the terrace surface. We selected the wide paved surface because such surfaces are usually characterized by low erosion rates and are thus well suited for surface exposure dating (e.g., van der Woerd *et al.*, 1998, 2006; Mériaux *et al.*, 2004; Matmon *et al.*, 2009).

Sampling and measurements

We sampled 7 well embedded cobbles on terrace T5 (Figure 12). The 7 samples have close ^{10}Be concentrations on the order of 3×10^6 at/g quartz (Table 1). This high nuclide concentration, which is twice the concentration of samples Qi4-29-27 from 2 m depth in T7, suggest that 1) T7 must have been shielded quite rapidly after deposition and 2) the T5 terrace surface has never been shielded and 3) inheritance and/or erosion, if present, have similar effects on the samples of T5. We will use the weighted mean of the 7 sample concentrations (3.21 ± 0.30 x 10e6 at/g(qtz); Table 1) as the ^{10}Be nuclide concentration of terrace T5 surface.

3.2.3 Waligong terrace samples

Geomorphology

It is across the Waligong ranges that the Yellow River has cut its most impressive gorge over a length of 30 km and a total drop of water level of 200 m (Figures 2 and 3). Across the western Waligong, the Yellow River has carved a deep gorge with walls reaching about 500 m (Figures 3a, 3b). The flat top of the gorge mimics the overall shape of the western Waligong (Figures 4 and 5), and slopes towards the west into Longyangxia reservoir (Figure 2). In fact, in more details, the top of the gorge is formed by the progressive down cutting of the river resulting in abandonment of a sequence of strath terraces carved in the bedrock , which are covered by a thin deposit of fluvial gravel and cobbles (Figures 5 and 13). These terraces now slope towards the west indicating that the western Waligong is actively growing and has progressively back tilted the terraces. While the main terrace levels can be clearly depicted in the landscape (Figures 5c and 5d), their shape narrows near the gorge and their riser join with a low angle the gorge rims so that they become unclear near the gorge and we were unable to number and map them precisely.

Sampling and measurements

We sampled two sites on each side of the gorge (Figures 2 and 13), Waligong right bank (WRB) and Waligong left bank (WLB), located at 2680 and 2940 m a.s.l., respectively. Given the difficulties of terraces mapping near the gorge rim, these two sites are not located within the regional Gonghe basin terrace stratigraphy. Elevation only is not sufficient as we suspect uplift to have occurred since their abandonment (see below). At both sites we sampled the bedrock as well as the overlying cobbles, 4 samples at WLB and 8 samples at WRB (Figure 13, Table 1).

On terrace WLB, samples have ^{10}Be concentrations that range from 0,56 to 2.6x106 at/g(qtz) (Table 1). The lowest concentration (0,561x106 at /g(qtz)) is found in a piece of a highly fractured quartz vein sampled near the gorge cliff edge (sample Qi4-59, Figure 13a). Qi4-60 is a bedrock sample near the cliff edge and has a concentration of 1.82x106 at/g(qtz). Both remaining samples have higher concentrations, Qi4-62 is a protruding bedrock high (Figure 13a) and Qi4-61 is a cobble from the top of the terrace conglomerate cover (Figure 13a). We think that the average concentration of these two latter samples of 2.57±0.11 at/g(qtz) (Table 1) corresponds to the nuclide concentration accumulated since terrace abandonment and that the lower concentrations in the other samples are due to removal of the conglomerate cover and erosion of the fragile quartz vein outcrop.

On WRB terrace, samples have ^{10}Be concentrations that range from 1.2 to 1.9×10^6 at/g(qtz) (Table 1). The 35% difference in concentration among the WRB samples may be explained by the relative positions of the samples in the section sampled (Figures 13c and 13d). It appears that samples with the lowest concentration, Qi4-48 and Qi4-47 (Figure 11c) are bedrock samples close to the gorge cliff, which are no more covered by the terrace conglomerate. Sample Qi4-49 belongs to a bedrock high (Figure 13c) standing at the same level as the pebbly conglomerate top and show a similar ^{10}Be concentration as the 5 surface

cobbles Qi4-50 to 54 (Table 1). The distribution of concentrations of the WRB samples is thus best explained by removal of the conglomerate cover near the gorge cliff. The ^{10}Be concentration average of 1.89±0.02e6 at/g(qtz) of the 6 samples with highest concentrations correspond to the nuclides accumulated since terrace abandonment.

3.3 Age Modeling

Model age of T7

We modeled jointly the ^{10}Be concentration and the ^{26}Al/^{10}Be ratio in the depth profiles (e.g., Anderson *et al.,* 1996; Granger & Smith, 2000) considering a deposition scenario in three steps corresponding to the stratigraphy observed in the field (Figures 8 and 10). Modelling results are presented in Figure 10 and take into account progressive increase in muongenic production at depth following analytical solutions described in Granger & Smith (2000) and calibrated to our site (Table 2). Disregarding samples with large inheritance and the sand samples, model 1 is a best fit adjusting all the ^{26}Al/^{10}Be ratios, and models 2 and 3 are limiting models toward short and long exposure times, respectively. In general, both the ^{10}Be concentration and the values of the ^{26}Al/^{10}Be ratio imply shielding by the loess during more than 150 ka (model 1). Involving fast erosion rates of the loess (0.01 cm/yr, model 3) very long time of loess shielding may be implied (400 ka) with the necessity to have an original loess thickness reaching several tens of meters.

Because the 2 m-thick loess deposit on top of the terrace is a shielding factor for cosmic rays (factor of decrease in production rate amounts to about 6) (e.g., Hetzel *et al.,* 2004; Matmon *et al.,* 2008) we have to consider its mode and timing of deposition. The presence of a paleosol below the loess (Figure 8) implies that the terrace surface remained free of loess during a certain time, i.e., quasi without any shielding. Without independent chronological

constraints on the loess age, several loess deposition modes can be modelled. In the first mode, the 2 m-thick loess is deposited instantaneously (or rapidly compared to the age of the terrace), in the second mode it was deposited continuously during a certain time (Figure 10c). Some constraints can be added from additional observations in Gonghe and elsewhere. As we mentioned above, loess is absent on the lower Yellow River terraces across the Gonghe basin, particularly on T5, so that the age of T5 may be the time when loess deposition stopped in the area (see below). In addition, 1 to 2 m-high loess sections described in northern Tibet generally show progressively younger ages towards the top (e.g., Peltzer *et al.,* 1988; van der Woerd *et al.,* 2002; Hetzel *et al.,* 2004; Rhode *et al.,* 2007) over a time period of a few thousands of years. Another possible factor of shielding variation is involved if the loess cover is reworked by wind ablation implying a period of loess deposition followed by a period of loess erosion (model 3).

Assuming that sub-surface samples cannot loose any ^{10}Be, except by radioactive decay, the lowest concentrated and deepest samples in a depth-profile (below about 1.5 m, Anderson et al., 1996) determine the minimum inherited component of the samples. We have thus considered the inheritance given by sample Qi4-29-21 (i.e., 235000 at/g, Table 1) in most models, and show only one alternative model (model 2) with an inheritance of 445000 at/g fitting the profile to the two sand samples with the lowest concentration (Qi4-29-23 and 15; Figure 10, Table 2). Note that the present Yellow river is carrying sand that has a ^{10}Be concentration of about 300000 at/g quartz (Table 1; see also Harkins *et al*. 2007) that may be considered as the average inherited ^{10}Be component of the alluvial material transported by the river, assuming it is constant over time and not variable with material size.

While below the paleosol, the fits to the data mostly depends on the choice of the inheritance value, above the paleosol, the fits mostly depends on the onset of loess shielding (Figure 10a, Table 2). These models also show that, in all cases, deposition of conglomerate C2 occurred

shortly after deposition of conglomerate C1 (10 to 15 ka). Similarly, deposition of the loess cover occurred shortly (0 to 25 ka) after deposition of conglomerate C2.

As shown in Figure 10c (Table 2), when a long-lasting loess deposition process is considered, shielding starts to be efficient when this process last less than 20 ka. This implies, that shielding by the loess must have started a few thousands of years after the terrace has been abandoned and that the loess must have been deposited in a short time. Note that this is fully in agreement with the observation, that the terraces below T7 are not loess covered, so that they must have been abandoned after the loess deposition process ceased in the region and on T7 in particular.

Sample Qi4-29-1, sampled above the paleosol and below the loess may be used as an additional constraint. It is clearly a reworked cobble as it is not emplaced in a fluvial deposit, but it must have been reworked at the time of the formation of the paleosol and before being capped by the loess. As can be seen in Figure 10a, models that are adjusted to this sample imply a minimum exposure of C2 of 10-15 ka. The same duration would be needed to account for soil formation above C2 and some surface reworking. The ^{10}Be concentration of this sample implies exposition under the loess during 150 ka.

To summarize, T7, or more precisely the top C2 conglomerate may have been deposited about 200 ka, and definitively incised by the Yellow River after 150 ka, some time before the 2 m loess cap accumulated on top of C2.

Model age of T5

Without independent constraints on erosion and inheritance for terrace T5, these parameters have to be estimated. Inheritance may be taken similar as for terrace T7 (235000 to 445000 at/g quartz) or similar to the present Yellow River sand ^{10}Be concentration of about 300000 at/g quartz (Table 1). Regarding erosion, studies have been carried out in the Gonghe basin

following intensification of agriculture and its consequence on desertification. Using the ^{137}Cs technique to assess erosion in drylands and sand shifting areas, erosion rates of about 1-2 mm/yr have been estimated over the last ~40 years (Yan *et al*., 2002; Zhang *et al*., 2003). These values of erosion are rather high (Lal *et al*., 2003) and may only reflect the consequence of human activities. Lower values of 0.003-0.01 mm/yr were estimated for bedrock outcrops throughout Tibet (Lal *et al*., 2003). Again these values should be taken as maximum erosion rates for a flat alluvial terrace.

The average age of T5 calculated from $3.04\pm0.17\times10^6$ atoms/g is 106 ± 6 ka. Both the inheritance of 300000 at/g quartz and a maximum erosion rate of 0.002 mm/yr (Figure 14) imply subtractive and additive corrections of 15-20%, respectively. Without evidence that erosion rates may be larger, we thus conclude that the minimum age of T5 is 106 ± 15 ka.

Age model of Waligong

To calculate the age of the terraces we need to take into account the change in elevation due to their tectonic uplift (e.g., Hetzel *et al*., 2004; Ruszkiczay-Rüdiger *et al*., 2005a, 2005b) (Figure 15). Waligong Shan is composed of two sub-parallel ranges at the junction between the eastern termination of the Qinghainan and the Laji Shan closing the northeastern corner of the Gonghe basin (Figure 2). The western Waligong is a 15 km-wide and 50 km-long arcuate range trending roughly northwest-southeast (Figures 1 and 2). Its asymmetric topographic shape, with a steep northeast and eastern flank under the summital crest that reaches 3500 m a.s.l. above a west dipping thrust and a western flank that slopes about 3.5° westward, (Figure 4e) indicate that it is an east-vergent crustal anticline. The eastern Waligong is less elevated but larger (20-30 km), trends northwest –southeast and makes up the western limit of the Guide basin. Similarly to the western Waligong, it has a steep eastern rim marked by a thrust at its base (Pan, 1994) and grows as an east-vergent anticline (Figure 2). As can be seen

in the field (Figure 13) the strath terraces are carved into the Waligong Mesozoic granodiorite (Geological map of Qinghai, 1988).

A simple model (Figure 15) accounting for the tilt of the Waligong Shan and uplift of the terraces implies possible changes in elevation of 80 m for WRB terrace and of about 300 m for WLB terrace (Figure 15). For WRB, the in-situ production rate changes from 25.73 at/g/yr at 2600 m to 27.04 at/g/yr at 2680 m. This change in production rate of about 10 % remains small with regard to other uncertainties and may be neglected. For WLB the production rate change is more significant, varying from 26.6 at/g/yr at 2640 m to 31.93 at/g/yr at 2940 m, i.e. a change of 20 %. The real mean production rate of this terrace lies certainly between these end-values and we will take the mean between these bounds with a large error of 15%. The terrace ages are thus 74±10 ka for WRB and 90±15 ka for WLB. The maximum changes in elevation mentioned above imply maximum uplift rates for Waligong Shan between 1 and 3 mm/year.

However, this model does not take into account the low $^{26}Al/^{10}Be$ ratio (5.23±0.27) obtained for sample Qi4-62 (WRG), which is a bedrock sample near the gorge cliff (Figure 13). This ratio implies that the surface bedrock needs to be exposed a first time (first cosmonuclide accumulation), then shielded during several hundred thousands years (ratio decreases; Figure 11) and then re-exposed until present. The cobble cover, likely deposited by the river, covered the surface before being progressively eroded to the present state (Figure 13). The beryllium concentrations of the cobbles would thus reflect the exposure duration since the river left, but bedrock concentrations are not totally related to this last phase of aggradation and erosion. The surface would thus be exposed since ~80 ka. Initiation of uplift likely began shortly afterwards at a minimum rate of 0.2 mm/year. Despite the fact that the ^{10}Be concentrations of the cobbles are higher on WLB than on WRB because of their higher elevation and production rate, simple calculations show that this scenario would lead to ^{10}Be concentrations

close to 2.0×10^6 at both sites, with a difference of ~2.0×10^5 atoms instead of the ~6.0×10^5 measured (Table 1).

4) Discussion

4.1 Onset age of incision in the Gonghe Basin

Whether the beginning of river incision corresponds to the first appearance of the Yellow River in the basin is an open question. Terrace sequences along the Yellow River differ markedly from Gonghe to Lanzhou. As explained above, terraces in the different basins seem completely unrelated to each other (ages, loess thickness, elevations). We cannot simply rely on these terraces to compare our chronology in the Gonghe Basin, but the timing of river incision should be coherent between the different basins (Harkins *et al*., 2007).

Several authors have proposed that incision in the Gonghe Basin began at around 150 ka. (e.g., Li, 1991; Pan, 1994). Evidences for a major change along the Yellow River 150 ka ago have been summarized by Zhang *et al*. (2004). Periods of high regressive erosion from the Longyang gorges and the Sanmen gorges (in the middle reaches of the Yellow River north of the Ordos plateau, inset, Figure 1) are reported around that time (Zhang *et al*., 2000; Wang *et al*., 2002). This period of erosion in the Longyang gorges could have followed the folding of the fluvial sediments of the Gonghe formation (Li, 1991). An increased sedimentation in the marine delta of the river could be related to this period of high erosion and to the climate warming of MIS-5 (Imbrie *et al*., 1984).

However, it has been proposed that incision began around 500 (±200) ka ago in the Tongde Basin (Harkins *et al*., 2007; Craddock *et al*., 2010), following the last 1.8 Ma lacustrine deposit near the top of the section in Guide (Li *et al*., 1997). A direct implication is that incision in the Gonghe Basin began at the same time or before, but not after, which means that T7 must be much older than results from our investigations suggest. This can only be

achieved if a significant amount of erosion or a long period of shielding occurred and may imply that all terraces are significantly older. A 140 ka (OSL) terrace located 140 m above the Yellow River is located at an elevation of ~2830 m in the Tongde basin (Harkins *et al.,* 2007; Craddock *et al.,* 2010). For comparison, an equivalent terrace in the Gonghe Basin would be near by T1, which is expected to be much younger than 140 ka.

4.2 Incision rates of the Yellow River in the Gonghe Basin

Terrace ages are plotted against their elevation on figure 16. The minimum and maximum long-term incision rates are ~2 and ~6 mm/year, respectively, with a mean rate of ~4 mm/year. This mean rate fits well with the ages of T5 and T7. However, for all data it is needed to account for changes in the incision rate. The incision rate between the formation of T7 and T5 depends strongly on the age of T7, if erosion on T5 remains small. A period of high incision is needed between T5/WLB and WRB. The incision rate may have reached 9 mm/yr (10 mm/year maximum, if no elevation changes are taken into account for the Waligong terraces). Our data suggest that incision was first slow, then accelerated between ~100 and 50 ka, before slowing down again. Such fast incision would have favoured the steep Waligong gorges formation.

A mean incision rate of 4 mm/year is higher than those mentioned in other places along the Yellow River in the literature, 0.7 mm/yr since 70 ka near Lanzhou (Wang *et al.,* 2010), between 0.75 and 1 mm/yr since 166 ka near Linxia (Li *et al.,* 1997) for the downstream part, between 0.9 and 1.0 mm/yr for the last 140 ka in the Tongde Basin (Harkins *et al.,* 2007). But it is in agreement with the 6 mm/yr since 93 ka in the Guide Basin proposed by Pan (1994).

4.3 Climatic correlations and formation of the set of terraces

It is now recognized that climatic fluctuations play a key role in shaping fluvial terraces.

Correlation of terrace formation periods with climatic events is however not straightforward, because uncertainties inherent to the cosmogenic nuclides dating method often prevent from determining a precise correlation. Transitional periods between glacial and interglacial periods seem nevertheless to play a major role in forming fluvial terraces. These periods would be favorable for incision, while aggradation would occur during stable climatic phases, possibly both glacial and interglacial (e.g., Vandenberghe, 2003).

Loess in northeastern China was mainly deposited during glacial periods, while paleosols developed during interglacial phases, alternating loess and paleosol layers being correlated to climatic fluctuations (e.g., Ding *et al.,* 2002). The fact that T7 gravels are directly overlain by a paleosol and this paleosol by a loess cover suggests that this terrace was abandoned during a deglaciation period and covered by loess during an aposteriori glacial event (Pan *et al.,* 2009). No such climatic indicators are available for the other terraces, although it is reasonable to assume that their formation followed a similar process, i.e., a formation as a consequence of dry/cold to wet/warm climate transition.

The terraces in the Gonghe Basin could have been formed during glacial periods and abandoned at the transition with warmer periods, when the river high incision power enabled it to break dams formed by the Waligong Shan.

4.4 Evidence for a Gonghe-Guide-Qinghai paleo-lake

Small lakes can be found in several places in the present Gonghe basin (Figure 6); Chaka Lake, in the northwest, has a present elevation of 3060 m; Dalian Lake, at an elevation of 2850 m (Yan *et al*. 2002); Duolonggou lake, north of Gonghe city, at an elevation of 3194 m. Lacustrine sediments can be found at several places in the Gonghe basin and at Dalian Lake for instance. These small lakes and sediments may be remnants of a larger lake occupying the bottom of the Gonghe basin (Figure 17). Such a lake may have covered adjacent intra-

mountainous basins. It has been reported that sedimentary sequences in the Guide Basin were deposited under lacustrine conditions (Parés *et al.,* 2003; Fang *et al.,* 2005; Li *et al.*, 1997). Moreover, it is striking that the present level of the Qinghai Lake is exactly at the same altitude as Duolonggou lake and as T7 sampling site (3200 m). Qinghai lake exists since ~0.5 Ma (Yuan *et al.,* 1990) and its present maximum depth approximates 20 meters (Colman *et al.,* 2007). Reconstructions of Qinghai lake water level paleo-elevations lead to various chronologies (Colman *et al.,* 2007; Madsen *et al.,* 2008; Rhode *et al.,* 2010; Liu *et al.,* 2010). The lake reached a maximum elevation of 3260 m (palaeo-shorelines older than 30 ka) and its level was particularly high during the penultimate glacial maximum (~150 ka). Other lakes in the region seemingly experienced the same high-stand event, the nearest in distance being Gahai Lake in the Qaidam Basin (Fan *et al.,* 2010).

The Chinese literature discusses the existence of an eastern Qinghai paleo-lake covering the Qinghai, Gonghe, Xinghai and Xining basin (e.g., Pan, 1994). It is based on a possible stratigraphic continuity between sediments in the Guide and Qinghai Basin. Such a lake would have broken into several parts due to the recent tectonic activity. Tectonic activity along the Qinghainan Shan fault likely began at the end of the Miocene or at the beginning of the Pliocene (Métivier *et al.,* 1998; Meyer *et al.,* 1998; van der Woerd, 1998; Fang *et al.*, 2005; Lease *et al.*, 2007) separating the Qinghai and Gonghe Basin. A connection between the two basins was possible at the southeastern extremity of Qinghai Lake when the pass may have been at a lower elevation (present elevation: 3350 m). The Qinghai Basin and the western Gonghe Basin are now internally drained. Madsen *et al.* (2008) proposed that Qinghai Lake began to form during the Middle or Late Pleistocene when the Riyue Shan uplift separated the Qinghai Basin from the Yellow River drainage system. Uplifting mountain ranges crossing the river course would have acted as boundaries for the eastern Qinghai paleo-lake, near the Longyang gorges (Gonghe Basin exit), Shanba gorges (Guide

Basin exit) or Jishi Gorges (Xunhua Basin exit) (Figure 17). The change from a lacustrine to a fluviatile environment would in this case correspond to the breaching of the topographic barriers and emplacement of the modern course of the Yellow River across the basins (Pares *et al.,* 2003; Craddock *et al.*, 2010).

However, no large lacustrine deposit can be found at present to attest more clearly the existence of such a lake, in particular at our sampling site of T7. Processes that lead to the formation of the wide paleo-regional base-level around 3200 m and of lakes present at this elevation stills need to be investigated, as well as the possible past connections between the different basins.

5) Conclusion

The Gonghe Basin is one of the widest basins of northeastern Tibet. It contains noteworthy wide terraces that testify to an important and recent water level decrease. Our results indicate that terraces were formed at the transition between glacial and interglacial periods. The upper one probably dates from the penultimate glacial maximum (MIS-6; Imbrie *et al.*, 1984). Obtained ages show that incision occurs at a mean rate of ~4 mm/year. Higher incision rates during some periods may be related to Waligong Shan uplift, although the tectonic signal remains difficult to separate from the river incision. Our results highlight the consequences of mountain growth and the interplay between tectonic and climatic processes in building the Tibetan Plateau. We provide chronological constraints supporting that this part of the plateau evolved rapidly in recent time from an internally drained but interconnected set of closed basins to an externally river drained plateau margin.

Acknowledgements

Field access and field trip support was provided by Institute of Tibetan Plateau Research, Chinese Academy of Sciences, Beijing, and the Chinese Earthquake Administration, Beijing, and its local bureau in Xining. We acknowledge support from INSU-CNRS (programmes Relief de la Terre), from CNES-SPOT Image (Tectoscope program, image acquired through ISIS program). The ^{10}Be measurements were performed at the ASTER AMS French national facility (CEREGE, Aix-en-Provences), which is supported by the INSU-CNRS, the French Ministry of Research and Higher Education, IRD, and CEA. Two measurements were also made at Center for Accelerator Mass Spectrometry at Lawrence Livermore National Laboratory. We thank Ecole et Observatoire des Sciences de la Terre (Strasbourg, France) and Université de Strasbourg for support and making possible the operation of the cosmogenic laboratory of Institut de Physique du Globe de Strasbourg (UMR 7516) and Laboratoire d'Hydrogéologie et de Géochimie de Strasbourg (UMR 7517).

References

Anderson, R.S., J.L. Repka and G.S. Dick, 1996. Explicit treatment of inheritance in dating depositional surfaces using in situ ^{10}Be and ^{26}Al, *Geology*, **24**, 47-51.

Balco, G., Stone, J., Lifton, N. & Dunai, T. 2008. A complete and easily accessible means of calculating surface exposure ages or erosion rates from ^{10}Be and ^{26}Al measurements. *Quaternary geochronology*, **3**, 174-495.

Balco, G. 2009. ^{26}Al-^{10}Be exposure age/erosion rate calculators: update from v. 2.1 to V. 2.2. World Wide Web Address: http://hess.ess.washington.edu/math/docs/al_be_v22/al_be_docs.html.

Benn, D. and Owen, L.A., 1998. The role of the Indian summer monsoon and the mid-latitude westerlies in Himalayan glaciation: review and speculative discussion. *Journal of the Geological Society,* **155**, 353-363.

Bierman, P.R., 1994. Using in-situ cosmogenic isotopes to estimate rates of landscape evolution: a review from the geomorphic perspective, *Journal of Geophysical Research*, **99**, 13885-13896.

Chen, Y.T., L.S. Xu, X. Li, and M. Zhao, 1996. Source process of the 1990 Gonghe, China, earthquake and tectonic stress field in the northeastern Qinghai-Xizang (Tibetan) plateau, Pure and Applied Geophysics, **146**, 697-715.

Clark, M.K., L.M. Schoenbohm, L.H. Royden, K.X. Whipple, B.C. Burchfiel, X. Zhang, W. Tang, E. Wang, L. Chen, 2004. Surface uplift, tectonics, and erosion of eastern Tibet from large-scale drainage patterns, *Tectonics*, **23**, TC1006, doi:10.1029/2002TC001402.

Colman, S. M., Yu, S.-Y., An, Z. & Henderson, A. C. G. 2007. Late Cenozoic climate changes in China's western interior: a review of research on Lake Qinghai and comparison with other records, *Quaternary Science Reviews*, **26**, 2281-2300.

Craddock, W.H., E. Kirby, N.W. Harkins, H. Zhang, X. Shi, J. Liu, 2010. Rapid fluvial incision along the Yellow River during headward integration, *Nature Geoscience*, doi:10.1038/NGEO777.

Ding, Z. L., Derbyshire, E., Yang, S. L., Yu, Z. W., Xiong, S. F. & Liu, T. S. 2002. Stacked 2.6-Ma grain size record from the Chinese loess based on five sections and correlation with the deep-sea $\delta^{18}O$ record. *Paleoceanography*, **17**(3), doi:10.1029/2001PA000725.

Domroes, M. and G. Peng, 1988. The Climate of China. Springer, Berlin. 361 pages.

England, P. C. & Houseman, G. A. 1986. Finite strain calculations of continental deformation: 2. Comparison with the India-Asia collision zone. *Journal of Geophysical Research,* **91**, 3664-3676, doi:10.1098/rsta.1988.0135

Fan, Q.S., Lai, Z. P., Long, H., Sun, Y. J. & Liu, X. J. 2010. OSL chronology for lacustrine sediments recording high stands of Gahai Lake in Qaidam Basin, northeastern Qinhai-Tibetan Plateau. *Quaternary Geochronology,* **5**, 223-227.

Fang, X., Garzione, C., Van der Voo, R., Li, J., Fan, M., 2003. Flexural subsidence by 29 Ma on the NE edge of Tibet from the magnetostratigraphy of Linxia Basin, China. *Earth and Planet. Sci. Lett.*, **210**, 545-560.

Fang, X., Yan, M., van der Voo, R., Rea, D. K., Song, C., Parés, J. M., Gao, J., Nie, J. & Dai, S. 2005. Late Cenozoic deformation and uplift of the NE Tibetan Plateau: evidence from high-resolution magnetostratigraphy of the Guide Basin, Qinghai Province, China. *GSA Bulletin*, **117**, 1208-1225.

Fluteau, F., G. Ramstein, and J. Besse, 1999. Simulating the evolution of the Asian and African monsoons during the past 30 Myr using an atmospheric general circulation model. *J. Geophys. Res.*, **104**(D10), 11,995–12,018.

Fothergill, P. A. & Ma, H. 1999. Preliminary observations on the geomorphic evolution of the

Guide Basin, Qinghai Province, China: implications for the uplift of the northeast margin of the Tibetan Plateau. *In*: Smith, B. J., Whalley, W. B. & Warke, P. A. (eds) *Uplift, erosion and stability: perspectives on long-term landscape development*. Geological Society, London, Special Publications, **162**, 183-200.

Frankel, K.L., 2010, Terrestrial cosmogenic nuclide geochronology data reporting standards needed, *EOS, Transactions, American Geophysical Union*, **91**, no. 4, 31-32.

Gao, H., Liu, X., Pan, B., Wang, Y., Yu, Y. & Li, J. 2008. Stream response to Quaternary tectonic and climatic change: evidence from the upper Weihe River, central China. *Quaternary International*, **186**, 123-131.

Gaudemer, Y., P. Tapponnier and D. L. Turcotte, 1989. River offsets across active strike-slip faults, *Annales Tectonicae*, III, n°2, 55-76.

Gaudemer, Y., P. Tapponnier, B. Meyer, G. Peltzer, Guo Shunmin, Chen Zhitai, Dai Huagung and I. Cifuentes, 1995. Partitioning of crustal slip between linked, active faults in the eastern Qilian Shan, and evidence for a major seismic gap, the "Tianzhu gap", on the Western Haiyuan Fault, Gansu (China). *Geophysical J. International*, **120**, 599-645.

Gosse, J. C. & Philips, F. M. 2001. Terrestrial in situ cosmogenic nuclides: theory and applications. *Quaternary Science Reviews*, **20**, 1475-1560.

Granger, D.E., A.L. Smith, 2000. Dating buried sediments using radioactive decay and muogenic production of 26Al and 10Be, *Nucl. Inst. Meth. Phys. Res.,* **B172**, 822-826.

Harkins, N., Kirby, E., Heismath, A., Robinson, R. &Reiser, U. 2007. Transient fluvial incision in the headwaters of the Yellow River, northeastern Tibet. *Journal of Geophysical Research*, **112**, F03S04, doi:10.1029/2006JF000570.

Hetzel, R., Tao, M., Stokes, S., Niedermann, S., Ivy-Ochs, S., Gao, B., Strecker, R. & Kubik, P. 2004. Late Pleistocene/Holocene slip rate of the Zhangye thrust (Qilian Shan,

China) and implications for the active growth of the northeastern Tibetan Plateau. *Tectonics*, **23**, TC6006, doi:10.1029/2004TC001653.

Houseman, G. & England, P. 1993. Crustal thickening versus lateral expulsion in the Indian-Asian continental collision. *Journal of Geophysical Research*, **98**, 12233-12249.

Imbrie, J., Hays, J. D., Martinson, D. G., McIntyre, A., Mix, A. C., Morley, J. J., Pisias, N. G., Prell, W. L. & Shackelton, N. J. 1984. The orbital theory of Pleistocene climate: support from a revised chronology of the $\delta^{18}O$ record. *In*: Berger, A., Imbrie, J., Hays, J., Kukla, G. & Saltzman, B. (eds) *Milankowitch and Climate*. Reidel, the Netherlands, 269-305.

Joussaume, S., 1999. Climat d'hier à demain, CNRS Edition, CEA, pp. 143.

Kohl, C. P. & Nishiizumi, K. 1992. Chemical isolation of quartz for measurements of *in-situ*-produced cosmogenic nuclides. *Geochimica et Cosmochimica Acta*, **56**, 3583-3587.

Lal, D., Harris, N. B. W., Sharma, K. K., Gu, Z., Ding, L., Liu, T., Dong, W., Caffee, M. W., Jull, A. J. T. 2003. Erosion history of the Tibetan Plateau since the last interglacial: constraints from the first studies of cosmogenic ^{10}Be from Tibetan bedrock. *Earth and Planetary Science Letters*, **217**, 33-42.

Lease, R.O., D.W. Burbank, G.E. Gehrels, Z. Wang, D. Yuan, 2007. Signatures of moutain building: Detrital zircon U/Pb ages from northeastern Tibet, Geology, 35, 1239-242.

Le Dortz, K., Meyer, B., Sébrier, M., Nazari, H., Braucher, R., Fattahi, M., Benedetti, L., Foroutan, M., Siame, L., Bourlès, D., Talebian, M., Bateman, M. D. & Ghoraishi, M. 2009. Holocene right-slip rate determined by cosmogenic and OSL dating on the Anar fault. *Geophysical Journal International*, doi:10.1111/j.1365-246X.2009.04309.x.

Li, J. 1991. The environmental effects of the uplift of the Qinghai-Xizang Plateau. *Quaternary Science Reviews*, **10**, 479-483.

Li, J.-J., Fung, X.-M., van der Voo, R., Zhu, J.-J., Mac Niocaill, C., Ono, Y., Pan, B.-T., Zhang, W., Wang, J.-L., Sasaki, T., Zhang, Y. T., Cao, J.-X., Kang, S.-C., Wang, J.-M. 1997. Magnetostratigraphic dating of river terraces: rapid and intermittent incision by the Yellow River of the northeastern margin of the Tibetan Plateau during the Quaternary, *Journal of Geophysical Research*, **102**, 10121-10132.

Lister, G.S., K. Kelts, K. Chen, J. Yu and F. Niessen, 1991. Lake Qinghai, China : closed-basin lake levels and the oxygen isotope record for ostracods since the latest Pleistocene, *Paleogeography, Paleoclimatology, Paleoecology*, 84, 141-162.

Liu, X. J., Lai, Z. P., Fan, Q. S., Long, H. & Sun, Y. J. 2010. Timing for high lake levels of Qinghai Lake in the Qinghai-Tibetan Plateau since the last interglaciation based on quartz OSL dating. *Quaternary Geochronology*, **5**, 218-222.

Liu-Zeng, J., Tapponnier, P., Gaudemer, Y. & Ding, L. 2008. Quantifying landscape differences across the Tibetan plateau: implications for topographic relief evolution. *Journal of Geophysical Research*, **113**, F04018, doi:10.1029/2007JF000897.

Lu, H., Wang, X., An, Z., Miao, X., Zhu, R., Ma, H., Li, Z., Tan, H., Wang, X. 2004. Geomorphologic evidence of phased uplift of the northeastern Qinghai-Tibet Plateau since 14 million years ago. *Science in China, Ser. D Earth Sciences*, **47**, 822-833.

Madsen, D. B., Haizhou, M., Rhodes, D., Brantigham, P. J., Forman, S. L. 2008. Age constraints on the late Quaternary evolution of Qinghai Lake, Tibetan Plateau, *Quaternary Research*, **69**, 316-325.

Matmon, A., Simhai, O., Amit, R., Haviv, I., Porat, N., McDonald, E., Benedetti, L., Finkel, R. 2009. Desert pavement-coated surfaces in extreme deserts present the longest-lived landforms on Earth. *Geological Society of America Bulletin*, **121**(5/6), 688-697, doi:10.1130/B26422.1.

Mériaux, A.-S., Ryerson, F. J., Tapponnier, P., Van der Woerd, J., Finkel, R. C., Xu, X.,

Xu, Z. & Caffee, M. W. 2004. Rapid slip along the central Altyn Tagh Fault: Morphochronologic evidence from Cherchen He and Sulamu Tagh, *Journal of Geophysical Research*, **109**, B06401.

Mériaux, A.-S., Tapponnier, P., Ryerson, F. J., Xu, X., King, G., van der Woerd, J., Finkel, R. C., Li, H., Caffee, M. W., Xu, Z. & Chen, W. 2005. The Aksay segment of the Northern Altyn Tagh fault : tectonic geomorphology, landscape evolution and Holocene slip-rate. *Journal of Geophysical Research*, **110**, B04404.

Métivier, F., Gaudemer, Y., Tapponnier, P & Meyer, B. 1998. Northeastward growth of the Tibet Plateau deduced from balanced reconstruction of two depositional areas: the Qaidam and Hexi Corridor basins, China. *Tectonics*, **17**, 823-842.

Meyer, B., Tapponnier, P., Bourjot, L., Métivier, F., Gaudemer, Y., Peltzer, G., Guo, S. & Chen, Z. 1998. Crustal thickening in Gansu-Qinghai lithospheric mantle subduction and oblique, strike-slip controlled growth of the Tibet Plateau. *Geophysical Journal International*, **135**, 1-47.

Nishiizumi, K., Imamura, M., Caffe, M., Southon, J., Finkel, R. & McAnich, J. 2007. Absolute calibration of ^{10}Be AMS standards. *Nuclear Instruments and Methods in Physics Research B*, **258**, 403-413.

Oskin, M., Peng, L., Shelef, E., Strane, M., Gurney, E;, Singer, B. & Zhang, X. 2008. Elevated shear zone loading rate during an earthquake cluster in eastern California. *Geology*, **36**(6), 507-510, doi:10.1130/G24814A.1.

Pan, B. 1994. Research upon the geomorphologic evolution of the Guide Basin and the development of the Yellow River. *Arid Land Geography*, **7**, 43-50.

Pan, B., Burbank, D., Wang, Y., Wu, G., Li, J. & Guan, Q. 2003. A 900 ka record of strath terrace formation during glacial-interglacial transitions in northwest China. *Geology*, **31**(11), 957-960.

Pan, B., Su, H., Hu, Z., Hu, X., Gao, H., Li, J. & Kirby, E. 2009. Evaluating the role of climate and tectonics during non-steady incision of the Yellow River: evidence from a 1.24 terrace record near Lanzhou, China. *Quaternary Science Reviews*, **28**, 3281-3290, doi:10.1016/j.quascirev.2009.09.003.

Parés, J. M., van der Voo, R., Downs, W. R., Yan, M. & Fang, X. 2003. Northeastward growth and uplift of the Tibetan Plateau: magnetostratigraphic insights from the Guide Basin. *Journal of Geophysical Research*, **108**, doi:10.1029/2001JB0012349.

Peltzer, G. & Tapponnier, P., 1988. Formation and evolution of strike-slip faults, rifts, and basins during the India-Asia collision: an experimental approach. *Journal of Geophysical Research,* **93**(B12), 15085-15117.

Qin, B., 1992. The hydrological characteristics and water budget of Qinghai lake drainage basin, *Chin. J. Oceanol. Limnol.*, **11**, 4, 314-320.

Qinghai Geological Bureau. 1988. *Geological Map of Qinghai-Xizang*, Ministry of Geology, Geological Press, Xining.

Repka, J. L., Anderson, R. S. & Finkel, R. C. 1997. Cosmogenic dating of fluvial terraces, Freemont River, Utah. *Earth and Planetary Science Letters*, **152**, 59-73.

Rhode, D., Z. Haiying, D.B. Madsen, G. Xing, P.J. Brantingham, H. Ma, J.W. Olsen, 2007. Epipaleolithic/early Neolithic settlements at Qinghai Lake, western China*, Journal of Archaeological Science*, **34**, 600-612.

Rhode, D., Haizhou, M., Madsen, D. B., Brantingham, P. J., Forman, S. L. & Olsen, J. W. 2010. Palaeoenvironmental and archaeological investigations at Qinghai Lake, western China: geomorphic and chronometric evidence of lake level history. *Quaternary International*, **218**, 29-44.

Royden, L., Burchfiel, B. C., King, R. W., Wang, E., Chen, Z. L., Shen, F. & Liu, Y. P. 1997. Surface deformation and lower crustal flow in eastern Tibet. *Science*, **276**, 788-790,

doi:10.1126/science.276.5313.788.

Ruszkiczay-Rüdiger, Zs., Fodor, L., Bada, G., Leél-Össy, Sz., Horváth, E. & Dunai, T. J. 2005a. Quantification of Quaternary vertical movements in the central Pannonian Basin: a review of chronologic data along the Danube River, Hungary. *Tectonophysics*, **410**, 157-172.

Ruszkiczay-Rüdiger, Zs., Dunai, T. J., Bada, G., Fodor, L. & Horváth, E. 2005b. Middle to late Pleistocene uplift rate of the Hungarian Mountain Range at the Danube Bend (Panonian Basin) using in situ produced ^{3}He. *Tectonophysics*, **410**, 173-187.

Schaller, M., F. von Blanckenburg, H. Veit, P.W. Kubik, 2002. Influence of periglacial cover beds on in situ-produced cosmogenic 10Be in soil sections. *Geomorphology*, **49**, 255-267.

Stone, J. O. 2000. Air pressure and cosmogenic isotopes production. *Journal of Geophysical Research*, **105**, 23753-23759.

Sun, J. 2005. Long-term fluvial archives in the Fen Wei Graben, central China, and their bearing on the tectonic history of the India-Asia collision system during the Quaternary. *Quaternary Science Reviews*, **24**, 1279-1286.

Tapponnier, P., Xu, Z. Q., Roger, F., Meyer, B., Arnaud, N., Wittlinger, G. & Yang, J. S. 2001. Oblique stepwise rise and growth of the Tibet Plateau. *Science*, **294**, 1671-1677.

Tapponnier, P., Peltzer, G., Armijo, R., Le Dain, A.-Y. & Cobbold, P. 1982. Propagating extrusion tectonics in Asia: new insights from simple experiments with plasticine. *Geology*, **10**, p 611-616.

Thompson, L. G., Yao, T., Davis, M. E., Henderson, K.A., Mosley-Thompson, E., Lin, P.-N., Beer, J., Synal, H.-A., Cole-Dai, J. & Bolzan, J. F. 1997. Tropical climate instability: the last glacial cycle from a Qinghai-Tibetan ice core. *Science*, **276**, 1821-1825.

Vandenberghe, J. 2003. Climate forcing of fluvial system development: an evolution of ideas. *Quaternary Science Reviews*, **22**, 2053-2060.

Van der Woerd, J. 1998. *Couplage cinématique entre décrochements et chevauchements actifs dans le nord du Tibet. Croissance du Plateau Tibétain*. PhD Thesis, University Paris VII.

Van der Woerd, J., Xu, X., Haibing, L., Tapponnier, P., Meyer, B., Ryerson, F., Meriaux, A.-S. & Xu., Z. 2001. Rapid active thrusting along the northwestern range front of the Tanghe Nan Shan (western Gansu, China). *Journal of Geophysical Research*. **106**(B12), 30475-30504.

Van der Woerd, J., Tapponnier, P., Ryerson, F. J., Mériaux, A.-S., Meyer, B., Gaudemer, Y., Finkel, R. C., Caffee, M. W., Zhao, G. & Xu, Z. 2002. Uniform postglacial slip-rate along the central 600 km of the Kunlun Fault (Tibet), from ^{26}Al, ^{10}Be and ^{14}C dating of riser offsets, and climatic origin of the regional morphology. *Geophysical Journal Internationl*, **148**, 356-388.

Van der Woerd, J., Y. Klinger, K. Sieh, P. Tapponnier, F.J. Ryerson, A.-S. Mériaux, 2006. Long-term slip rate of the southern San Andreas Fault from ^{10}Be-^{26}Al surface exposure dating of an offset alluvial fan. *Journal of Geophysical Research,* **111**, B04407, doi:10.1029/2004JB003559.

Wang, P., Jiang, H., Yuan, D., Liu, X. & Zhang, B., 2010. Optically stimulated luminescence dating of sediments from the Yellow River terraces in Lanzhou: tectonic and climatic implications. *Quaternary Geochronology*, **5**, 181-186.

Wang, S., Wu X., Zhang, Z., Jiang, F., Xue, B., Tong, G. & Tian, G. 2002. Sedimentary records of environmental evolution in the Sanmen Lake Basin and the Yellow River running through the Sanmenxia Gorges eastward into the sea. *Science in China (Series D)*, **47**, 596-608.

Xie, X. 2004. Late Cenozoic basin evolution along the Yellow River Corridor, Qinghai Province, China and the development of the NE Tibetan Plateau. *AAPG Foundation Project*.

Yan, M., Parés, J. M., van der Voo, R., Rea, D. K. & Fan, X. 2004. Pleistocene magnetostratigraphy of the Gonghe Basin, NE Tibetan Plateau: headward incision of the Yellow River after 1.8 Ma. American Geophysical Union, spring meeting 2004, abstracdt GP31A-17.

Yan, P., Shi, P., Gao, S., Chen, L., Zhang, X. & Bai, L. 2002. ^{137}Cs dating of lacustrine sediments and human impacts on Dalian Lake, Qinghai Province, China. *Catena*, **47**, 91-99.

Yuan, B. Y., Chen, K. Z., Bowler, J. M. & Je, S. S. 1990. The formation and evolution of Qinghai Lake. *Quaternary Sciences*, **3**, 233-243 (in Chinese with English abstract).

Zhang, C., Gong, J., Zou, X., Dong, G., Li, X., Dong & Z., Qing, Z. 2003. Estimates of soil movement in a study area in Gonghe Basin, north-east of Qinghai-Tibet Plateau. *Journal of Arid Environments*, **53**, 285-295.

Zhang, Z., Wang, S., Wu, X., Jiang, F. & Li, X. 2000. Age and environmental implications of the Sanmen Basin piercing in the middle reaches of Yellow River. *Journal of Geosciences of China*, **2**, 42-44.

Zhang, Z., Wang, S., Yang, X., Jiang, F., Shen, J. & Li, X. 2004. Evidence of a geological event and environmental change in the catchment area of the Yellow River at 0.15 Ma. *Quaternary International*, **117**, 35-40.

Zheng, D., Zhang, P., Wan, J., Li, C., Cao, J., 2003. Late Cenozoic deformation subsequence in northeastern margin of Tibet: Detrital AFT records from Linxia Basin. *Science in China, Series D*, **46**, 266-275.

Figures captions

Figure 1. Sismotectonic map of the upper reaches of the Yellow River across northeastern Tibet. Fault modified from van der Woerd (1998), Meyer *et al*. (1998), Tapponnier *et al*. (2001). Seismicity from Iris catalog, focal mechanisms from Harvard. Gonghe 1990 M 7 earthquake isoseismal from Chen *et al*. (1996). Topographic background is contours extracted from SRTM DEM with a 30sec precision.

Figure 2. (a) SPOT satellite image mosaic of eastern Gonghe basin. White rectangle is figure 2b. (b) CORONA image showing the northern part of the basin aross Yellow River terrace flights, Waligong Shan and Longyang gorge. c) Digital elevation model (SRTM, 90 m, GeomapApp) of most parts of the Gonghe, Guide and Qinghai Lake basins. Yellow River terraces clearly show up in central part of figure as wide fan shape stairs. Inset is elevation data histogram of same area. The tight peak of elevation around 3200 m a.s.l. is the wide plateau surface corresponding to surface elevation of the Gonghe and Qinghai Lake basins, as well as part of the Guide and Tongde basins. d) Geomorphological map of the Yellow River terraces in the eastern Gonghe basin. White filled circles are sampling site on terraces T7 and T5. (e) Topographic cross-section of terraces following black line of figure 2d (projection N85°E).

Figure 3. (a) Slope variations along the Yellow River. River slope reaches its maximum values (>0.5°) across the Longyang and Kongma gorges. (b) Profile of Yellow River bed from the southern Anyemaqen to Xunhua Basin. Red lines are active faults at basin margins (strike-slip, normal or reverse). Vertical scale is exaggerated 100 times. Profiles were extracted from SRTM DEM. River profile across Longyangxia Reservoir from Chinese 1:50000 topographic maps. Position and terrace ages upstream from Gonghe from Harkins *et*

al. (2007). (c) Enlarged Yellow River profile between Tongde and Xunhua, with projection of the Gonghe terraces (relative heights from figure 2), upper T7 regional top fill, and samples locations. Height of terraces in Guide basin from Fang *et al*. (2005). Colors of terrace threads in different basins are arbitrary.

Figure 4. (a) Field photo of the Longyang gorges, view towards the east. (b) Steep gorge cliff on right bank of river incising flat abraded bedrock surface, view towards the south. (c) Terrace T7/T6 riser inside Gonghe basin (see Figure 2), view towards the north. Riser forms a wind shelter where dunes accumulate (barkanes). (d) Yellow river gorge in the south of the Gonghe basin, view towards north. River can be seen cutting trough the sediment fill and northern bedrock sliver of Heka Shan (e.g., Métivier et al., 1998). Flat incised surface is level T7. (e) View to west at the steep thrust contact between the Mesozoic granodiorite of the western Waligong and the Tertiary red sandstones in the Yellow River gorge.

Figure 5. (a) Panoramic view of Waligong gorge. (b) View to west, towards Longyangxia Reservoir. In front, rim of bedrock strath can be seen. Note westward sloping flat top surface above the gorge. (c) View to east of stepped slope of western Waligong near the gorge that corresponds to the progressive entrenching and narrowing of the Yellow River bed. (d) View to west of the terraces in southwestern flank of Waligong Shan.

Figure 6. Google Earth view of the Gonghe and Qinghai basins with present lakes or lake remnants (salt flats, abandoned shore lines) highlighted.

Figure 7. (a) View towards south of terrace T7 surface, (see location in figure 2). Surface T7 merges smoothly with range slopes at the margin of the basin. (b) View towards north of T7

on the right bank of the Yellow River, in southern Gonghe basin. In front, gravel quarry that allowed access to first 10 meters of terrace deposit.

Figure 8. (a) The top 10 m of terrace T7 in a gravel quarry on the right bank of the Yellow River, north of Heka Shan (see location in figure 2). The terrace conglomerate is covered by a 2 m-thick loess deposit. Yellow vertical line (hanging tape) shows position of depth profile. Schematic section is shown on left with position of samples. Single pebbles, amalgamated samples and sand lenses were collected from 2 to 10 m depth. (b) Detail of paleosol between loess cover and conglomerate. (c) Detail of sand lenses.

Figure 9. Mass distribution plot (probability density function) of amalgamated pebbles of samples Qi4-29-27a, b, c and d collected about 2.1 ± 0.1 m deep below T7 surface. Number of pebbles, average mass and approximate size are indicated. Concentrations of ^{10}Be measured in amalgams are shown (see Table 1) together with weighted mean.

Figure 10. (a) Plot of ^{10}Be concentrations of sub-surface samples of terrace T7 (see Table 1). Schematic stratigraphy of the section is shown. (b) ^{26}Al/^{10}Be ratio as a function of depth for a subset of samples of figure 10a. Models 1, 2 and 3 are fitted to both the ^{10}Be and the ^{26}Al/^{10}Be ratio (see text and Table 2). (c) Models showing the impact of various loess accumulation scenarios, first number is duration of loess deposit, second number is duration of exposure at the end of loess deposit. Conglomerates C1 and C2 where exposed each during 15 ka (Table 2).

Figure 11. ^{26}Al/^{10}Be ratio versus ^{10}Be for a subset of samples from the depth profile of terrace T7 (Table 1).

Figure 12. (a) View to east of terrace T5 surface, showing a loose pavement of gravels and pebbles. Note absence of loess cover (see location in figure 2). At places, terrace T5 is covered by sand dunes and grass patches. Surface cobbles were collected for ^{10}Be cosmogenic dating in very flat areas with no sign of soil development or local incision. (b) to (h), close-up of cobbles sampled for surface exposure dating.

Figure 13. (a) View of Waligong left bank terrace (WLB) just above Longyang gorges (see figure 2 for location). The terrace is a smooth strath carved in granitic bedrock of Waligong Shan covered by a thin layer (> 1 m) of gravels and pebbles. Both granitic bedrock strath and overlaying pebbles were targeted for ^{10}Be exposure dating. (b) Schematic section with sample locations on WLB. (c) View of Waligong right bank (WRB) terrace with sample locations. Similarly to WLB, the strath terrace is smooth and covered by a thin layer of pebbles and cobbles. (d) Schematic section of WRB with sample locations. Samples Qi4-47 to -49 are bedrock, samples Qi4-50 to 54 are cobbles.

Figure 14. Minimum exposure age range of T5 and influence of erosion. Erosion of about 0.001 mm/yr cannot be excluded, but erosion of 0.003 mm/yr may be a maximum (see text for details).

Figure 15. (a) to (d) Schematic reconstruction of progressive incision of Yellow River across uplifting Waligong range. Phased incision leads to the formation of large stepped terraces across the basin, while strath terraces formed across Waligong bedrock are progressively uplifted and tilted. (e) Present-day section at same scale.

Figure 16. Incision rate of the Yellow River deduced from terrace ages and elevations. Coloured boxes are allowed age and elevation ranges. Yellow River elevation taken at Waligong gorges entrance (= WRB site). Several scenarios and associated incision rates are proposed. For Waligong terraces, rates are mean rates calculated from the middle of boxes. Maximum and mean total incision rates 6.0 mm/year and 4.0 mm/year, in orange.

Figure 17. Topographic contours at 3150, 3200 and 3250 m a.s.l. showing possible extensions of a regional paleolake or closed basin in the area of Qinghai and Gonghe basins before their separation due to lake capture by Yellow River and growth of the Qinghainan Shan. Lake surface elevation may have reached 3200-3250 m a.sl. This mapping, drawn from the present topography, does not account for large tectonic and morphologic changes.

Table 1. ^{10}Be and ^{26}Al analytical results of surface and sub-surface samples of the Yellow river terraces in the Gonghe basin..

Table 2. Depth profile model parameters (see Figure 10).

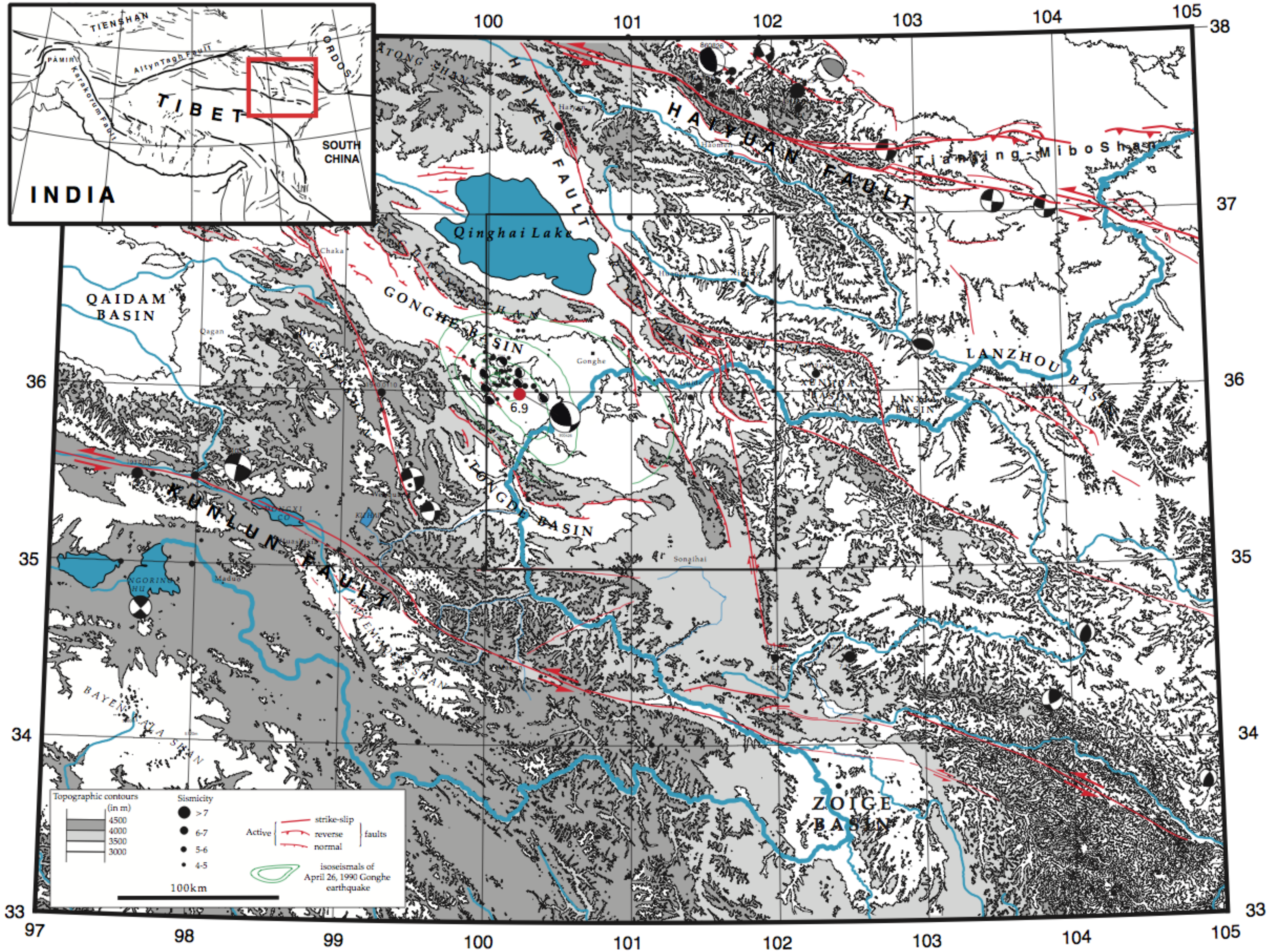
TIENSHAN
ALTYNTAGH FAULT
PAMIR
KARAKORUM FAULT
ORDOS
TIBET
SOUTH CHINA
INDIA
100
101
102
103
104
105
38
37
36
35
34
33
97
98
99
HAIYUAN FAULT
Qinghai Lake
QAIDAM BASIN
GONGHE BASIN
LANGDE BASIN
LANZHOU BASIN
ZOIGE BASIN
KUNLUN FAULT
6.9
Tianjing
MiboShan
Topographic contours (in m)
4500
4000
3500
3000
Sismicity
>7
6-7
5-6
4-5
Active
strike-slip
reverse
normal
faults
isoseismals of April 26, 1990 Gonghe earthquake
100km

Figure 1

(a)

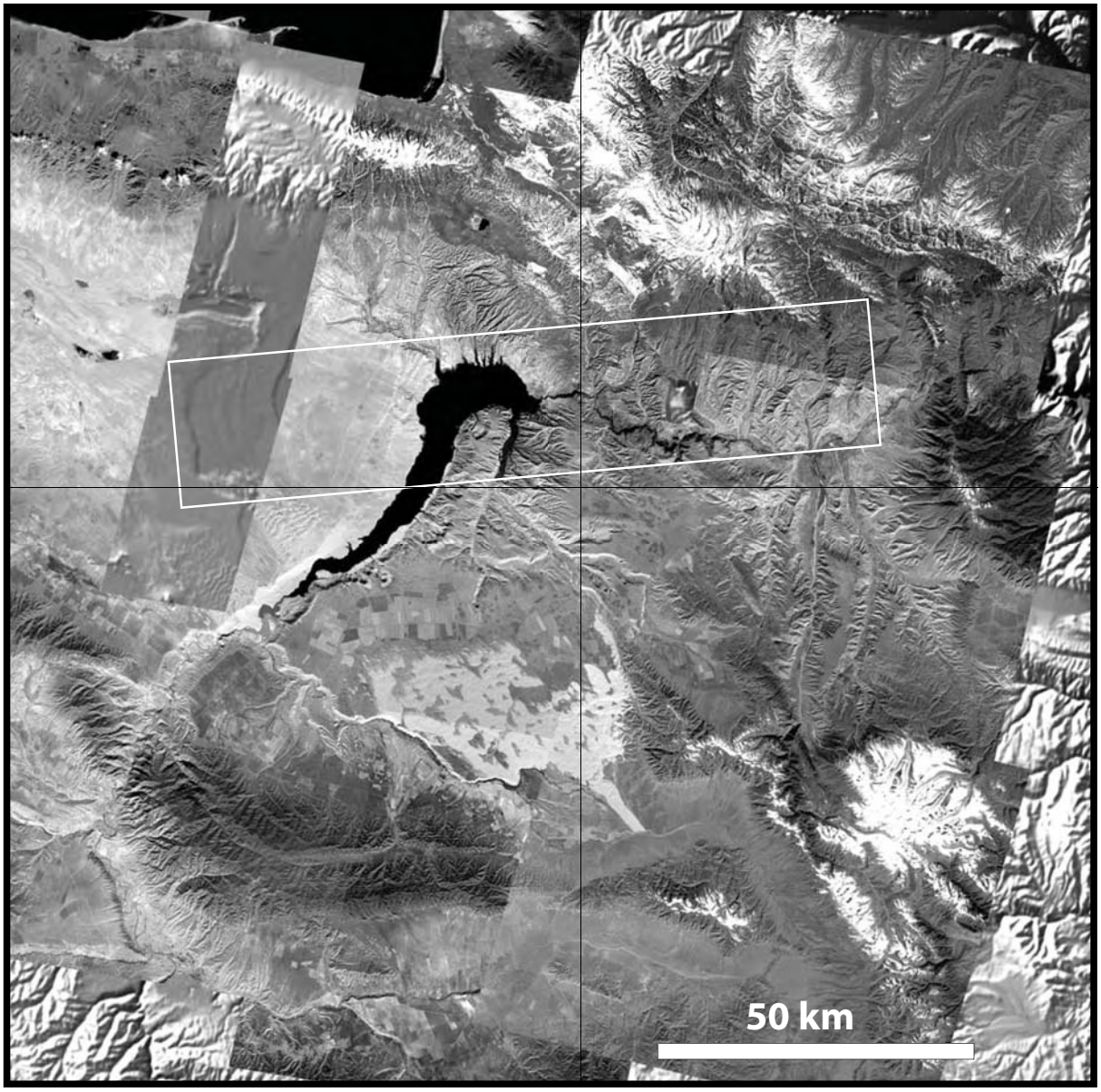

(b)

Figure 2ab

(c)

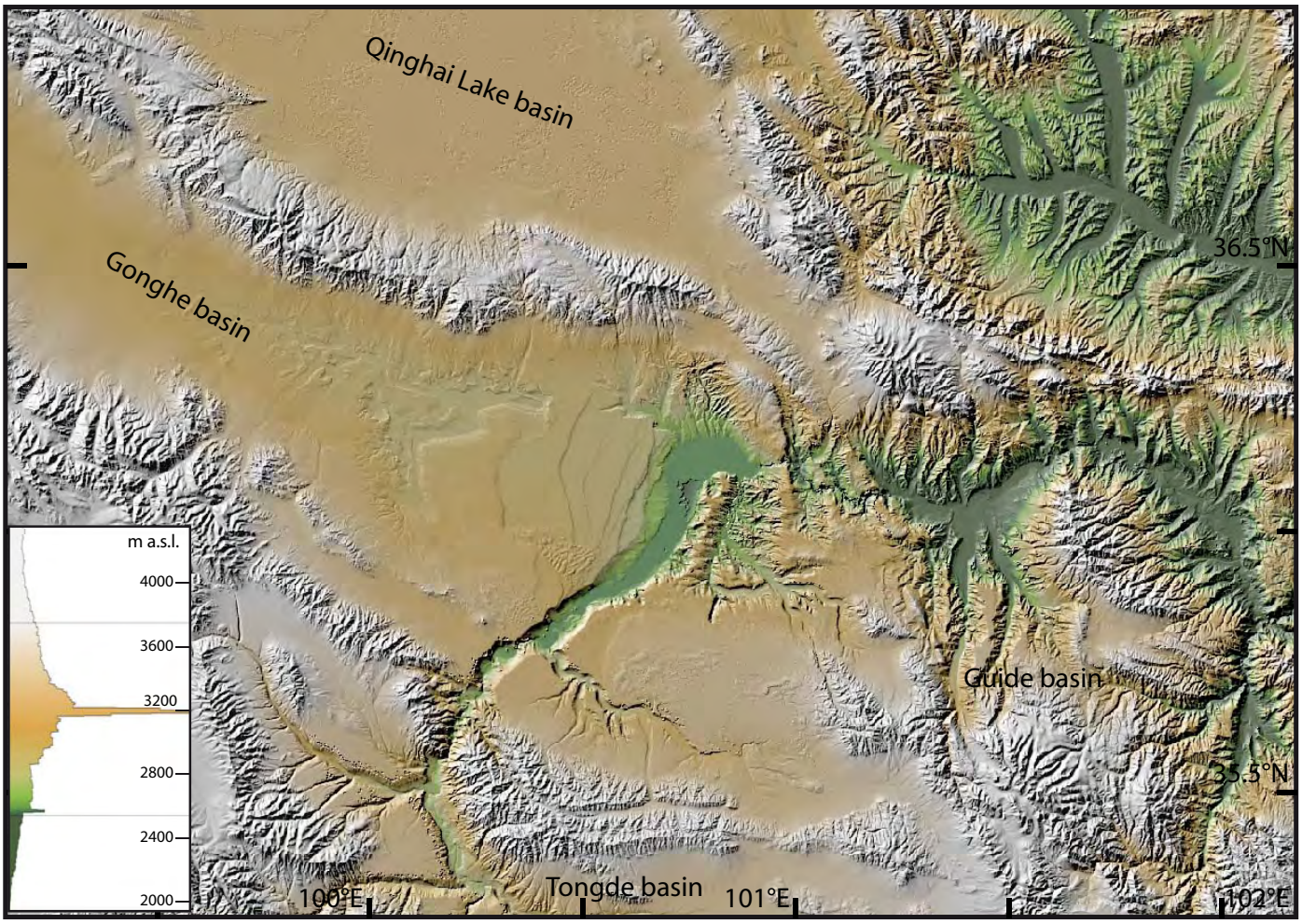
Qinghai Lake basin
Gonghe basin
Guide basin
Tongde basin
36.5°N
35.5°N
100°E
101°E
102°E
m a.s.l.
4000
3600
3200
2800
2400
2000

Figure 2c

(d)

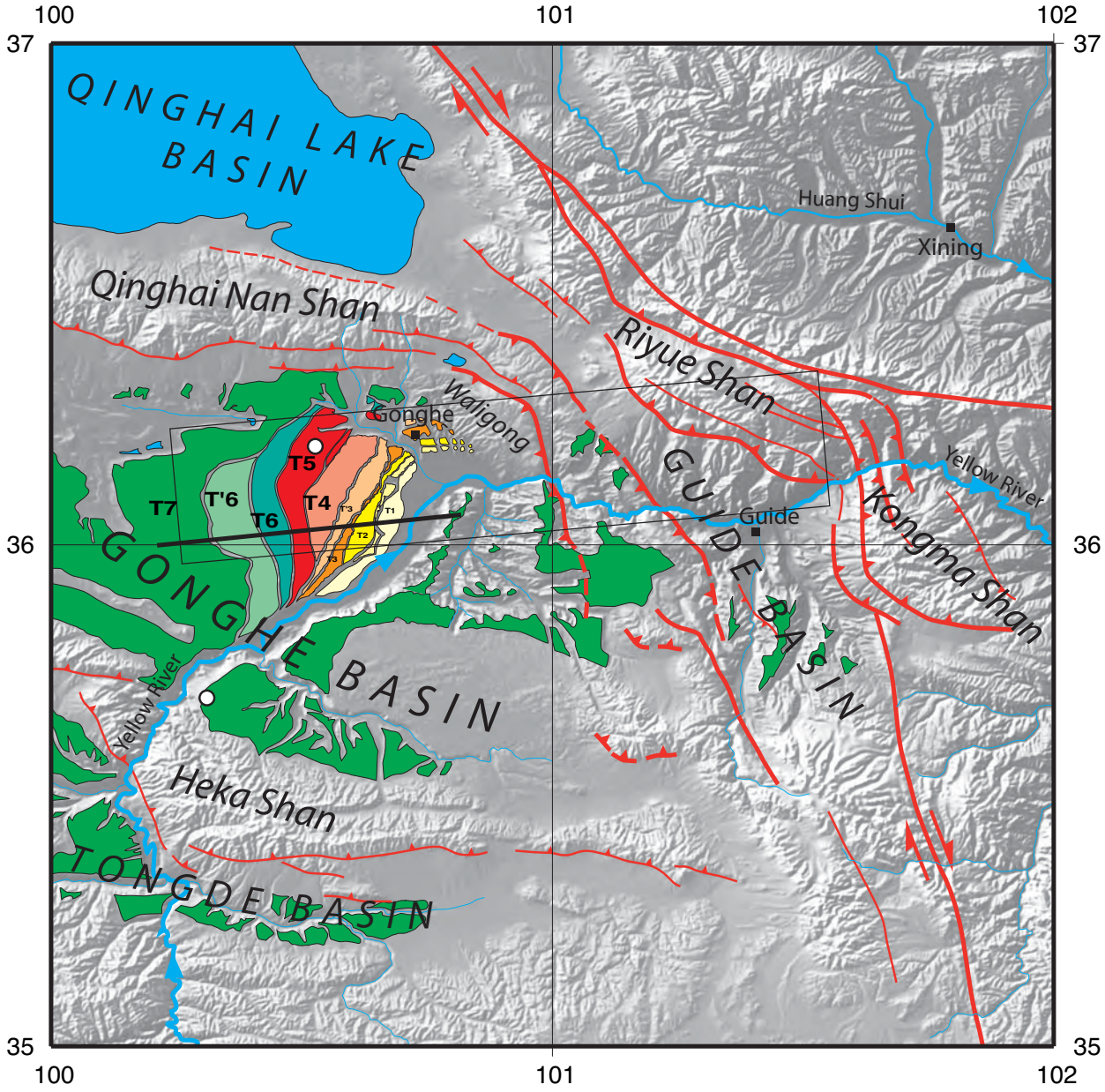

(e)

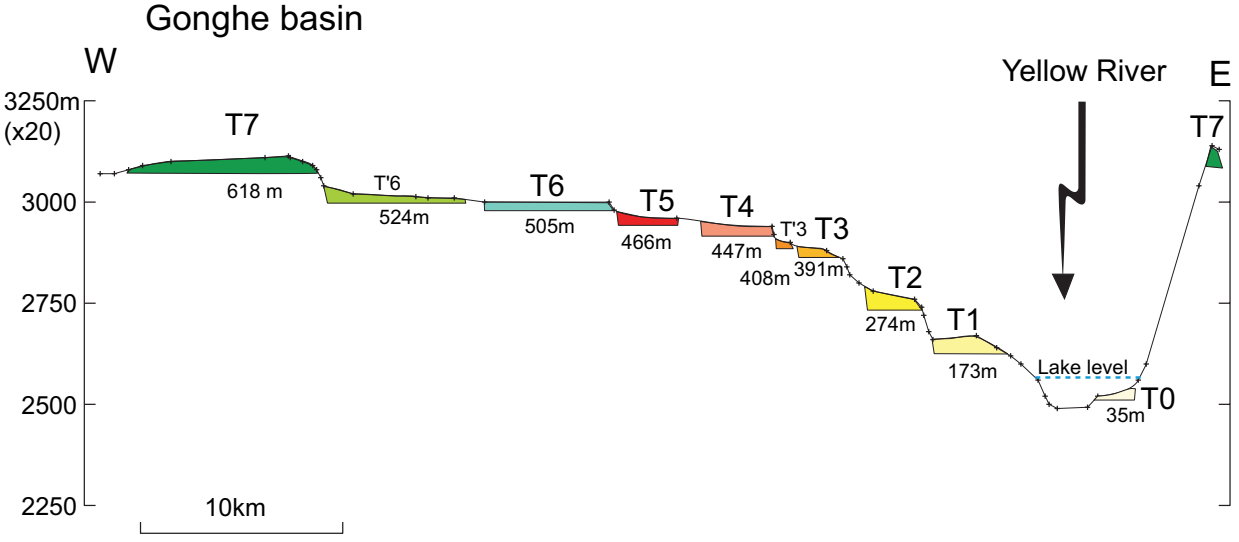

Figure 2de

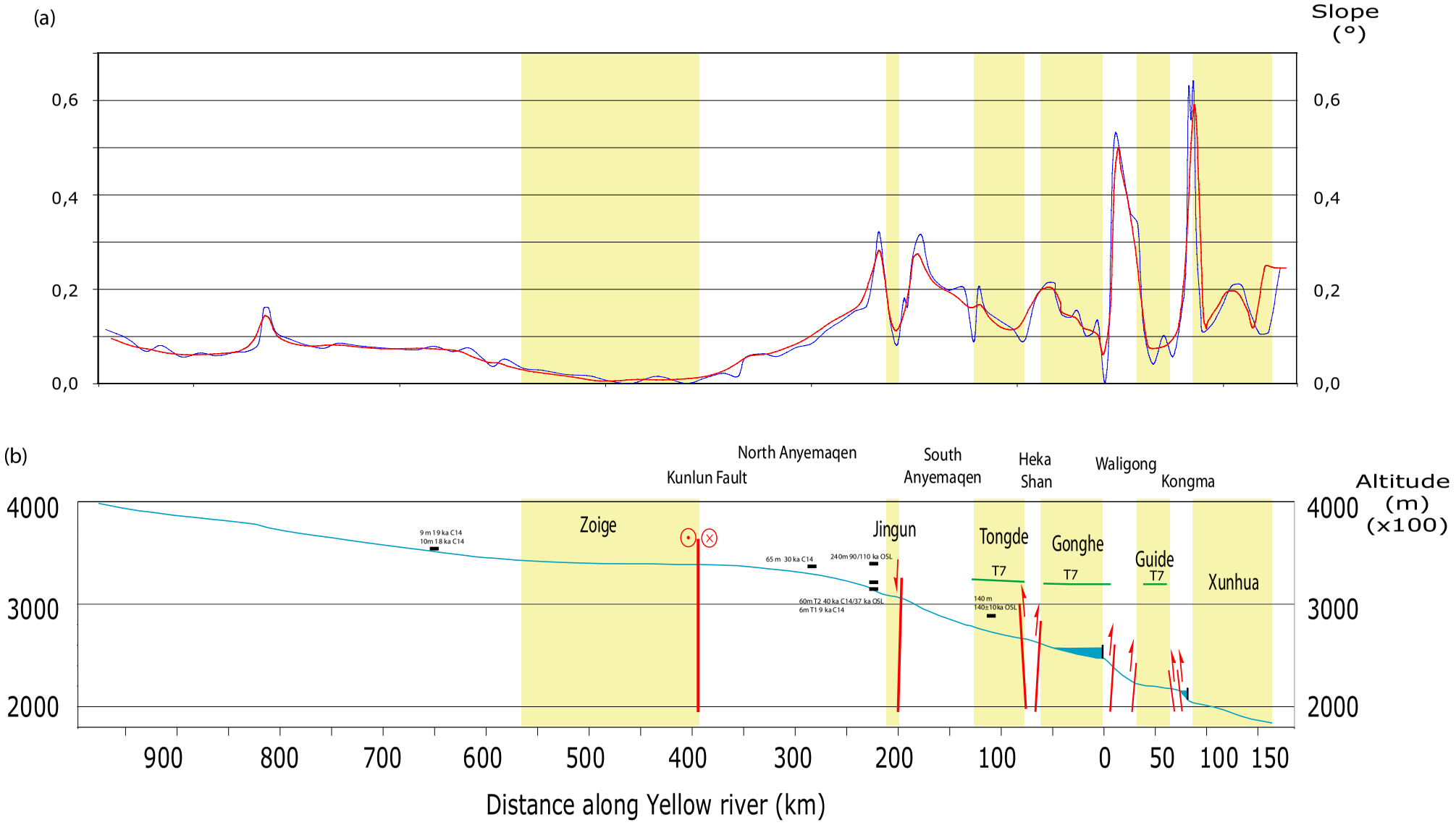
(a)
Slope (°)
0,6
0,4
0,2
0,0
(b)
North Anyemaqen
Kunlun Fault
South Anyemaqen
Heka Shan
Waligong
Kongma
Altitude (m) (x100)
4000
3000
2000
Zoige
Jingun
Tongde
Gonghe
Guide
Xunhua
T7
9 m 19 ka C14
10m 18 ka C14
65 m 30 ka C14
240m 90/110 ka OSL
60m T2 40 ka C14/37 ka OSL
6m T1 9 ka C14
140 m
140±10 ka OSL
900
800
700
600
500
400
300
200
100
0
50
100
150
Distance along Yellow river (km)

Figure 3ab

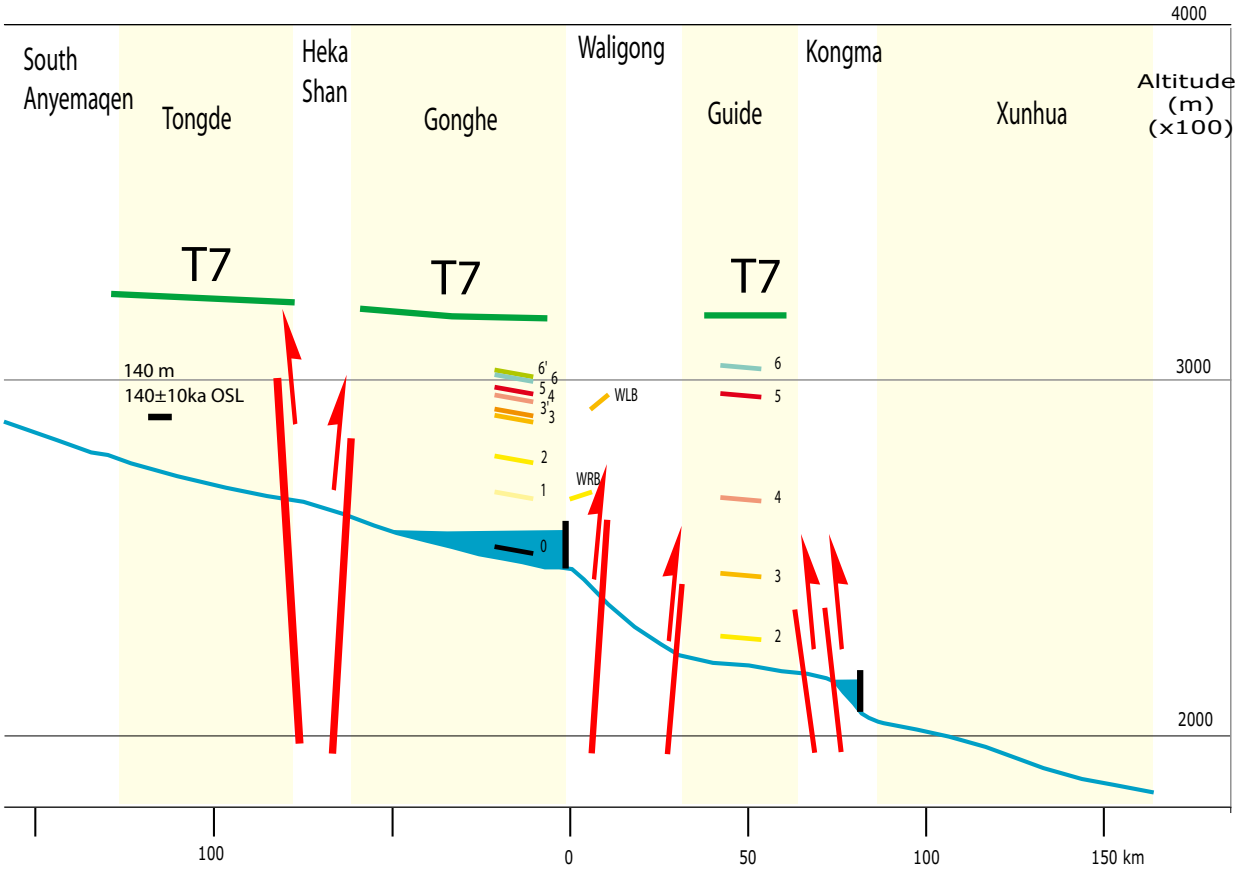
South
Anyemaqen
Tongde
Heka
Shan
Gonghe
Waligong
Guide
Kongma
Xunhua
Altitude
(m)
(×100)
4000
3000
2000
T7
T7
T7
140 m
140±10ka OSL
WLB
WRB
6'
6
5
4
3'
3
2
1
0
6
5
4
3
2
100
0
50
100
150 km

Figure 3c

(a)

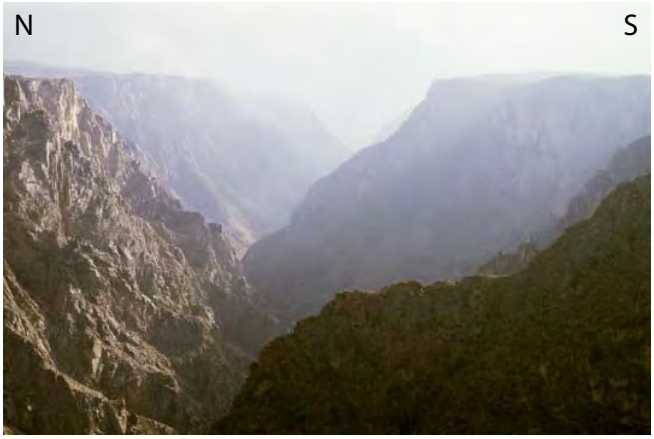

(b)

(c)

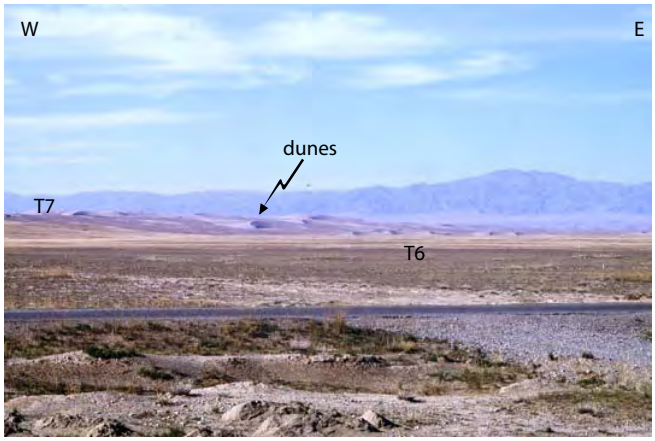

(d)

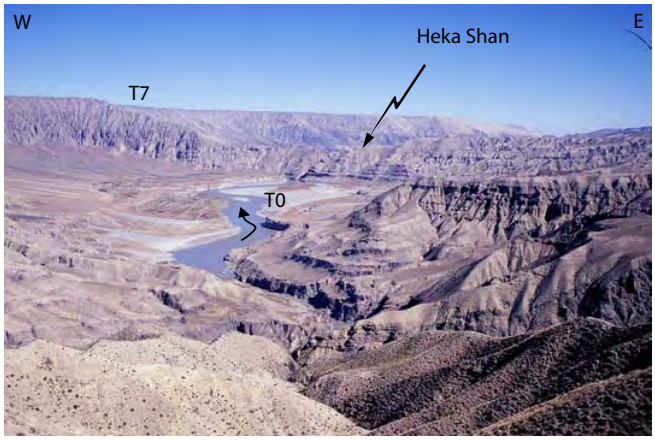

(e)

Figure 4

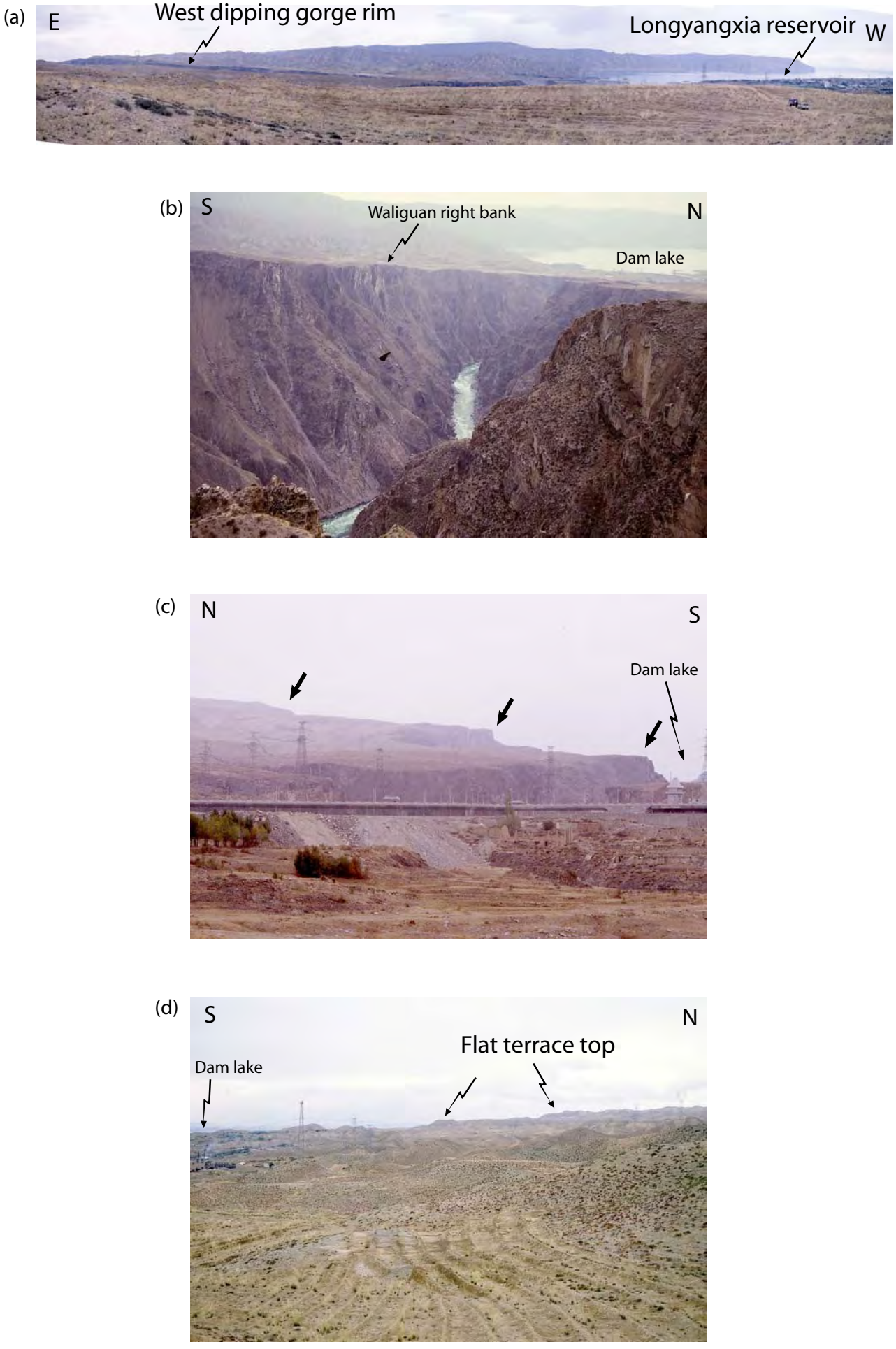
(a)
E
West dipping gorge rim
Longyangxia reservoir
W
(b)
S
Waliguan right bank
N
Dam lake
(c)
N
S
Dam lake
(d)
S
N
Flat terrace top
Dam lake

Figure 5

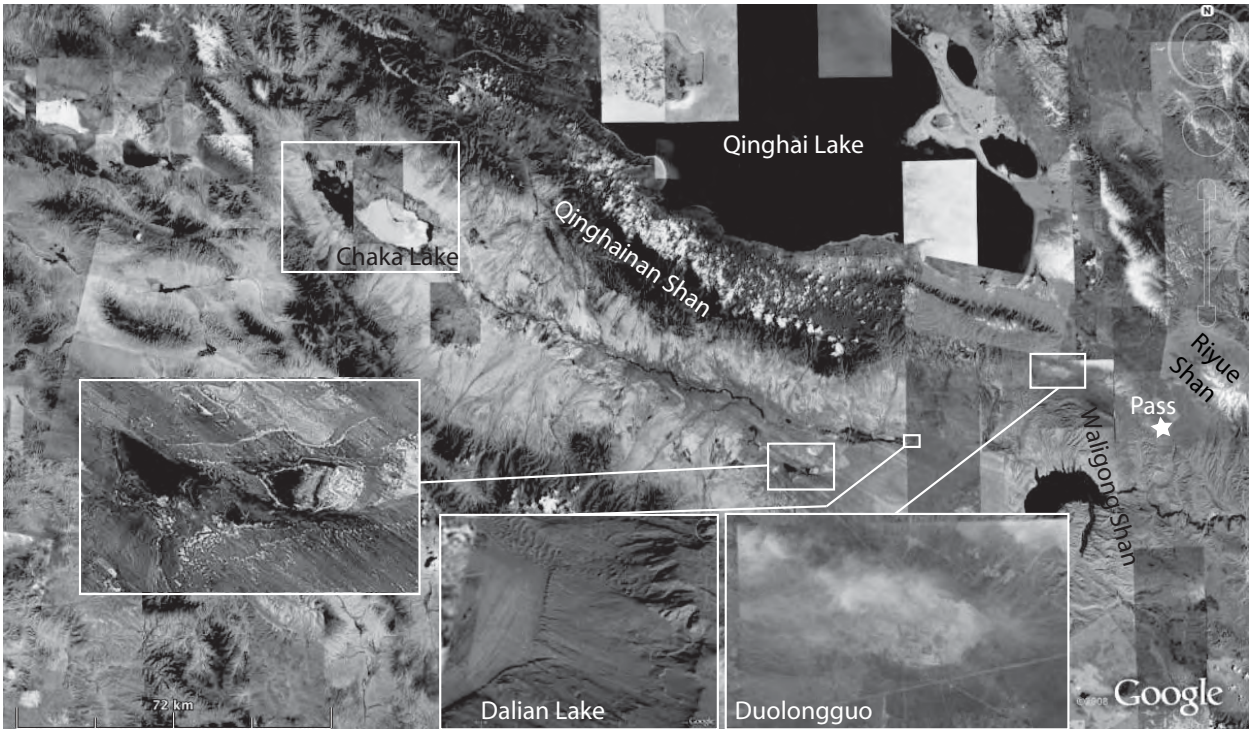
Qinghai Lake
Chaka Lake
Qinghainan Shan
Riyue Shan
Pass
Waligong Shan
72 km
Dalian Lake
Duolongguo
Google

Figure 6

(a)

(b)

Figure 7

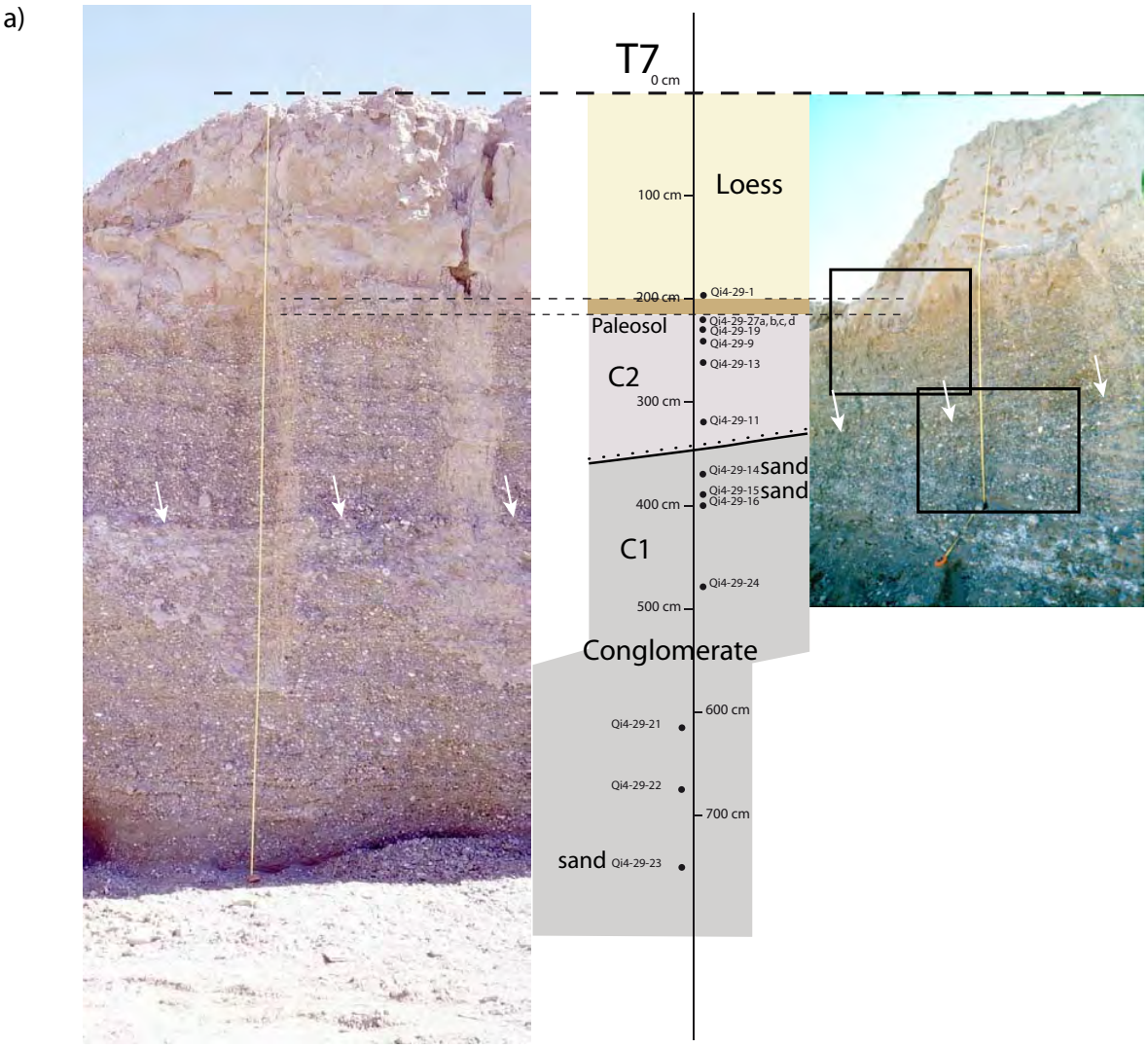
a)
T7
0 cm
100 cm
200 cm
300 cm
400 cm
500 cm
600 cm
700 cm
Loess
Paleosol
C2
C1
Conglomerate
sand
sand
Qi4-29-1
Qi4-29-27a, b, c, d
Qi4-29-19
Qi4-29-9
Qi4-29-13
Qi4-29-11
Qi4-29-14
Qi4-29-15
Qi4-29-16
Qi4-29-24
Qi4-29-21
Qi4-29-22
Qi4-29-23
b)
Qi4-29-1
25 cm
c)
25 cm
Qi4-29-14
5°
Qi4-29-15

Figure 8

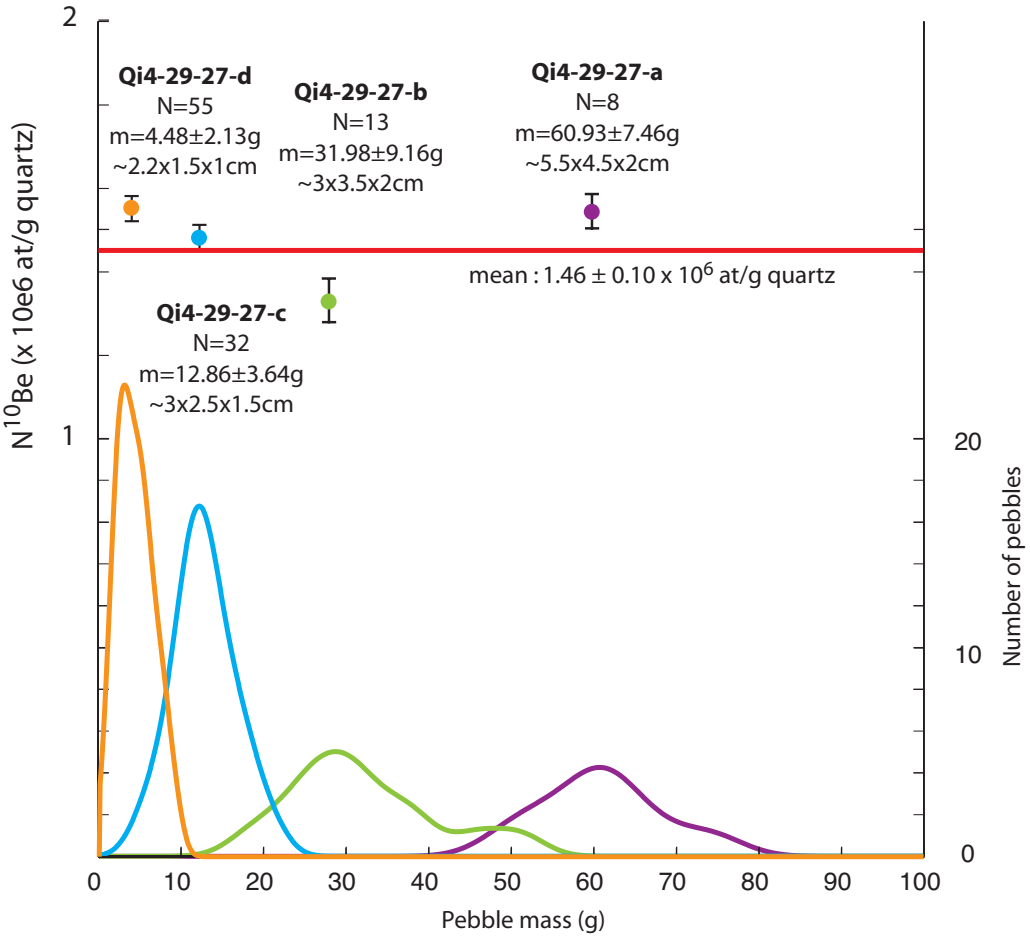
Qi4-29-27-d
N=55
m=4.48±2.13g
~2.2x1.5x1cm
Qi4-29-27-b
N=13
m=31.98±9.16g
~3x3.5x2cm
Qi4-29-27-a
N=8
m=60.93±7.46g
~5.5x4.5x2cm
mean : 1.46 ± 0.10 x 10^6 at/g quartz
Qi4-29-27-c
N=32
m=12.86±3.64g
~3x2.5x1.5cm
N 10Be (x 10e6 at/g quartz)
Number of pebbles
Pebble mass (g)
0
10
20
30
40
50
60
70
80
90
100
1
2
20
10
0

Figure 9

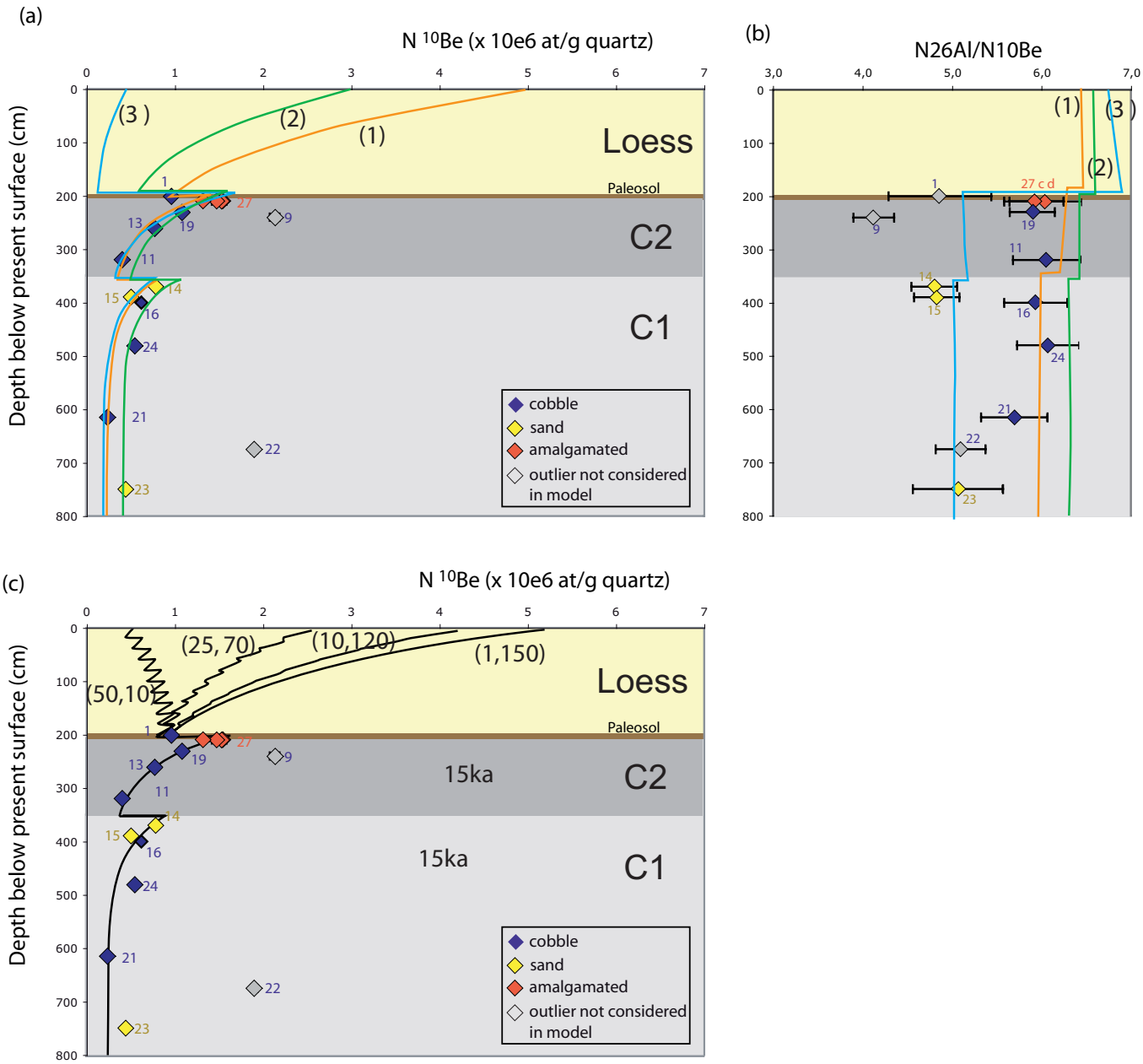

Figure 10abc

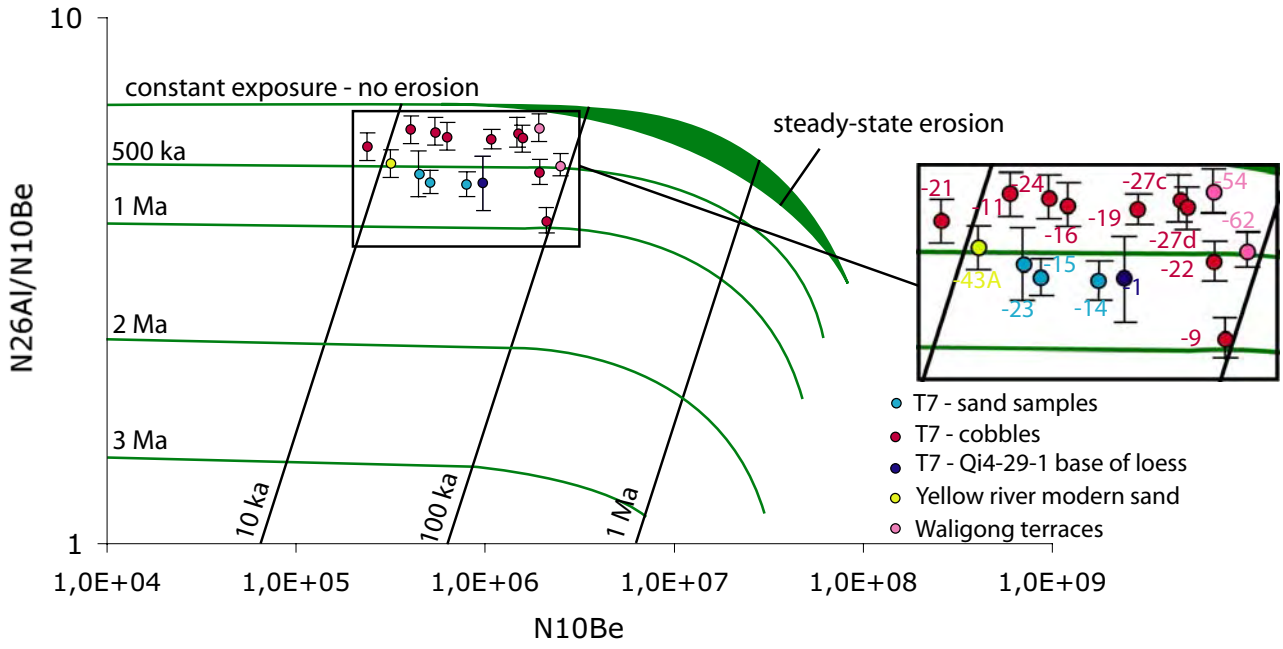
10
1
N26Al/N10Be
constant exposure - no erosion
steady-state erosion
500 ka
1 Ma
2 Ma
3 Ma
10 ka
100 ka
1 Ma
1,0E+04
1,0E+05
1,0E+06
1,0E+07
1,0E+08
1,0E+09
N10Be
-21
-11
-24
-16
-19
-27c
-27d
-54
-62
-22
-43A
-23
-15
-14
-1
-9
T7 - sand samples
T7 - cobbles
T7 - Qi4-29-1 base of loess
Yellow river modern sand
Waligong terraces

Figure 11

(a)

(b)

(c)

(d)

(e)

(f)

(g)

(h)

Figure 12

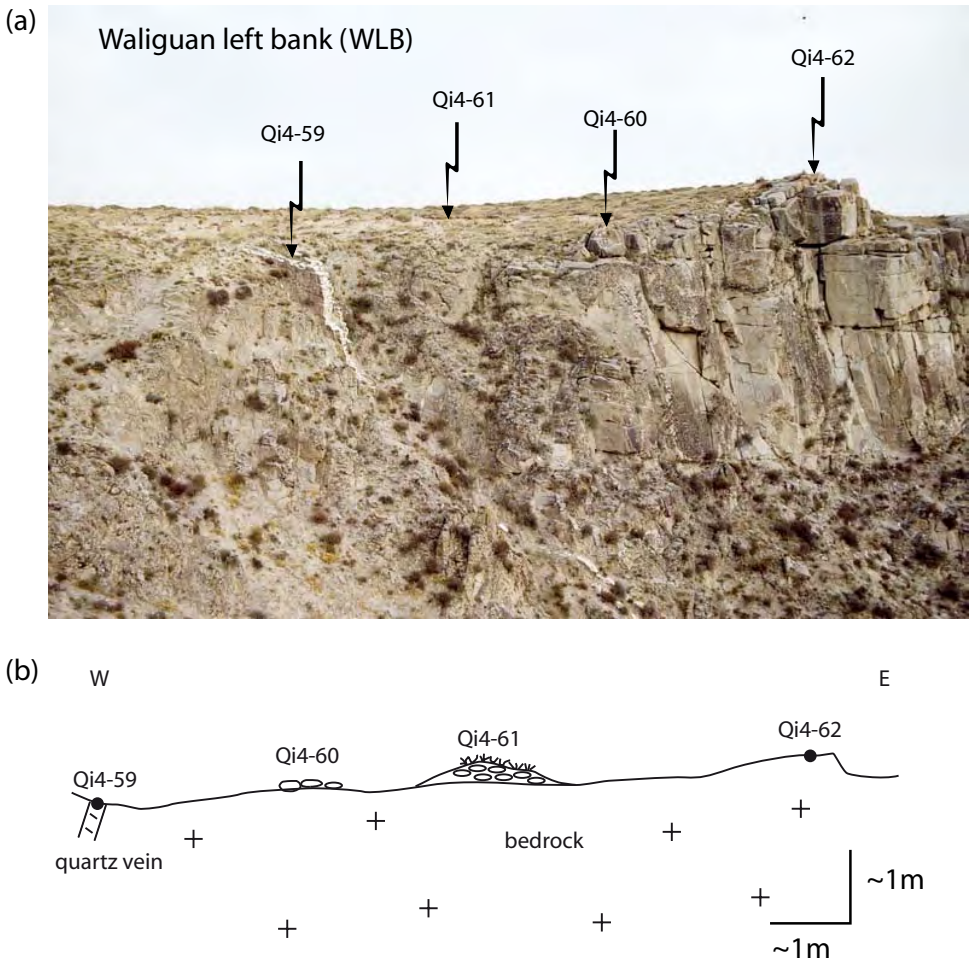
(a)
Waliguan left bank (WLB)
Qi4-59
Qi4-61
Qi4-60
Qi4-62
(b)
W
E
Qi4-59
Qi4-60
Qi4-61
Qi4-62
quartz vein
bedrock
~1m
~1m
(c)
(d)
S
N
Qi4-50 to 54
Qi4-49
Qi4-47
Qi4-48
cobbles
bedrock
Waliguan right bank (WRB)
~1m
~1m

Figure 13

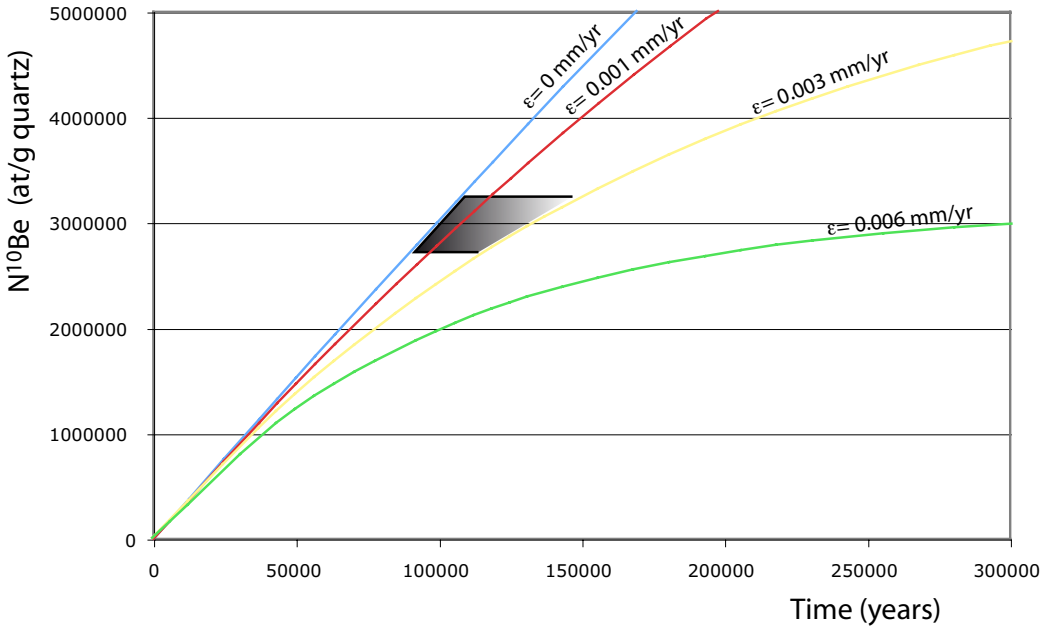
5000000
4000000
3000000
2000000
1000000
0
N10Be (at/g quartz)
0
50000
100000
150000
200000
250000
300000
Time (years)
ε= 0 mm/yr
ε= 0.001 mm/yr
ε= 0.003 mm/yr
ε= 0.006 mm/yr

Figure 14

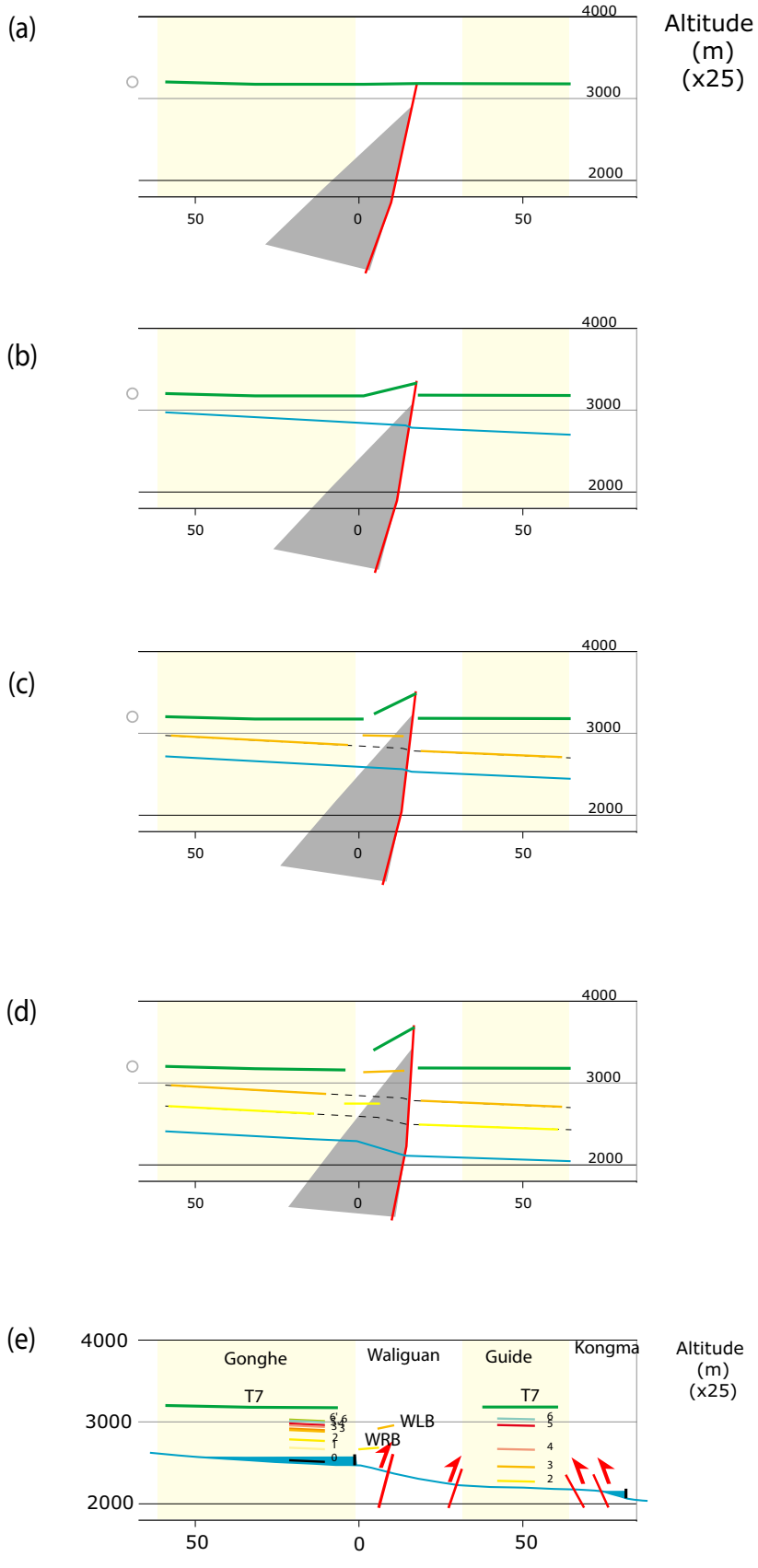
(a)
(b)
(c)
(d)
(e)
Altitude
(m)
(x25)
4000
3000
2000
50
0
50
Gonghe
Waliguan
Guide
Kongma
T7
WLB
WRB

Figure 15

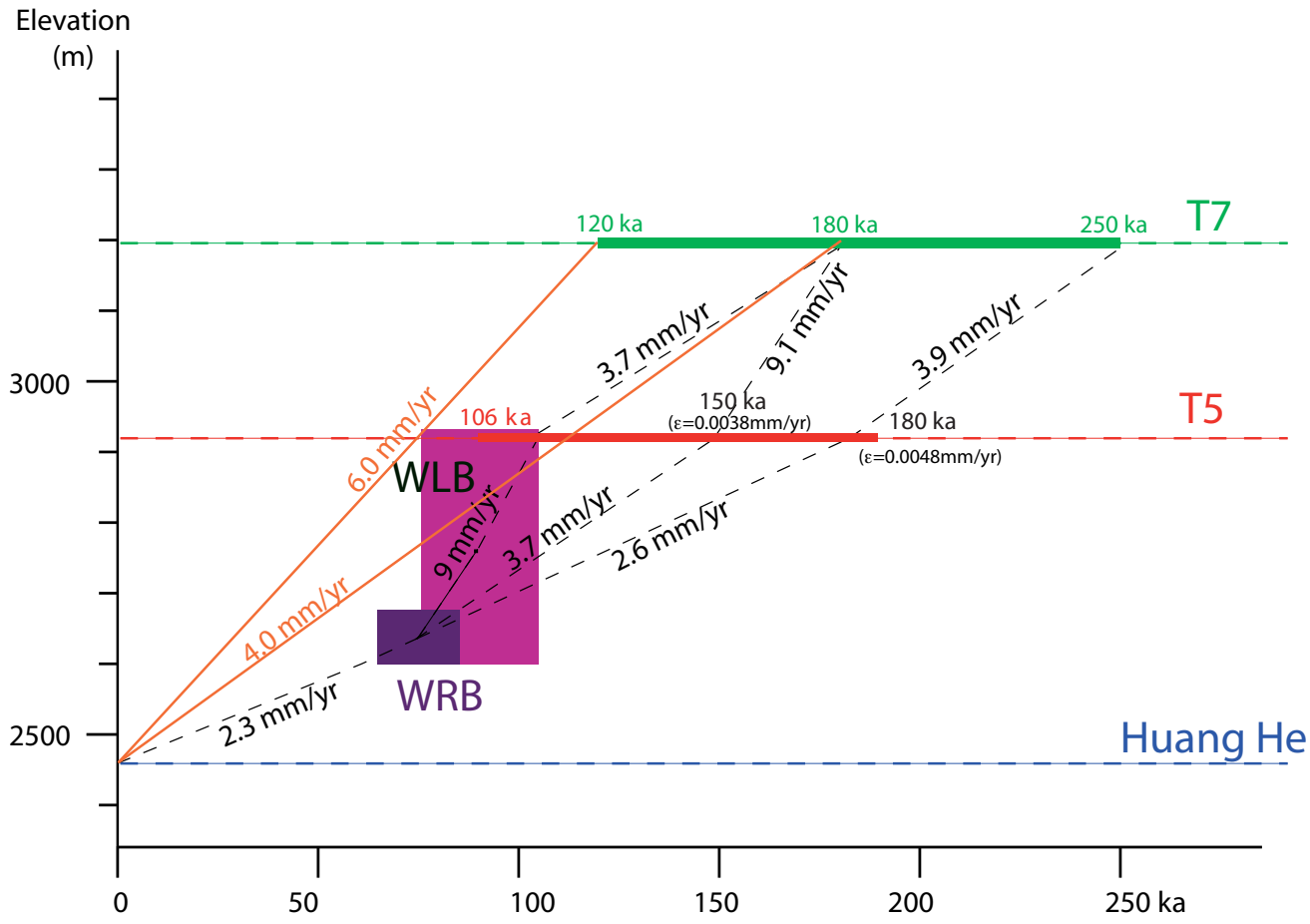
Elevation
(m)
3000
2500
0
50
100
150
200
250 ka
120 ka
180 ka
250 ka
T7
T5
106 ka
150 ka
(ε=0.0038mm/yr)
180 ka
(ε=0.0048mm/yr)
WLB
WRB
Huang He
6.0 mm/yr
4.0 mm/yr
3.7 mm/yr
9.1 mm/yr
3.9 mm/yr
9 mm/yr
3.7 mm/yr
2.6 mm/yr
2.3 mm/yr

Figure 16

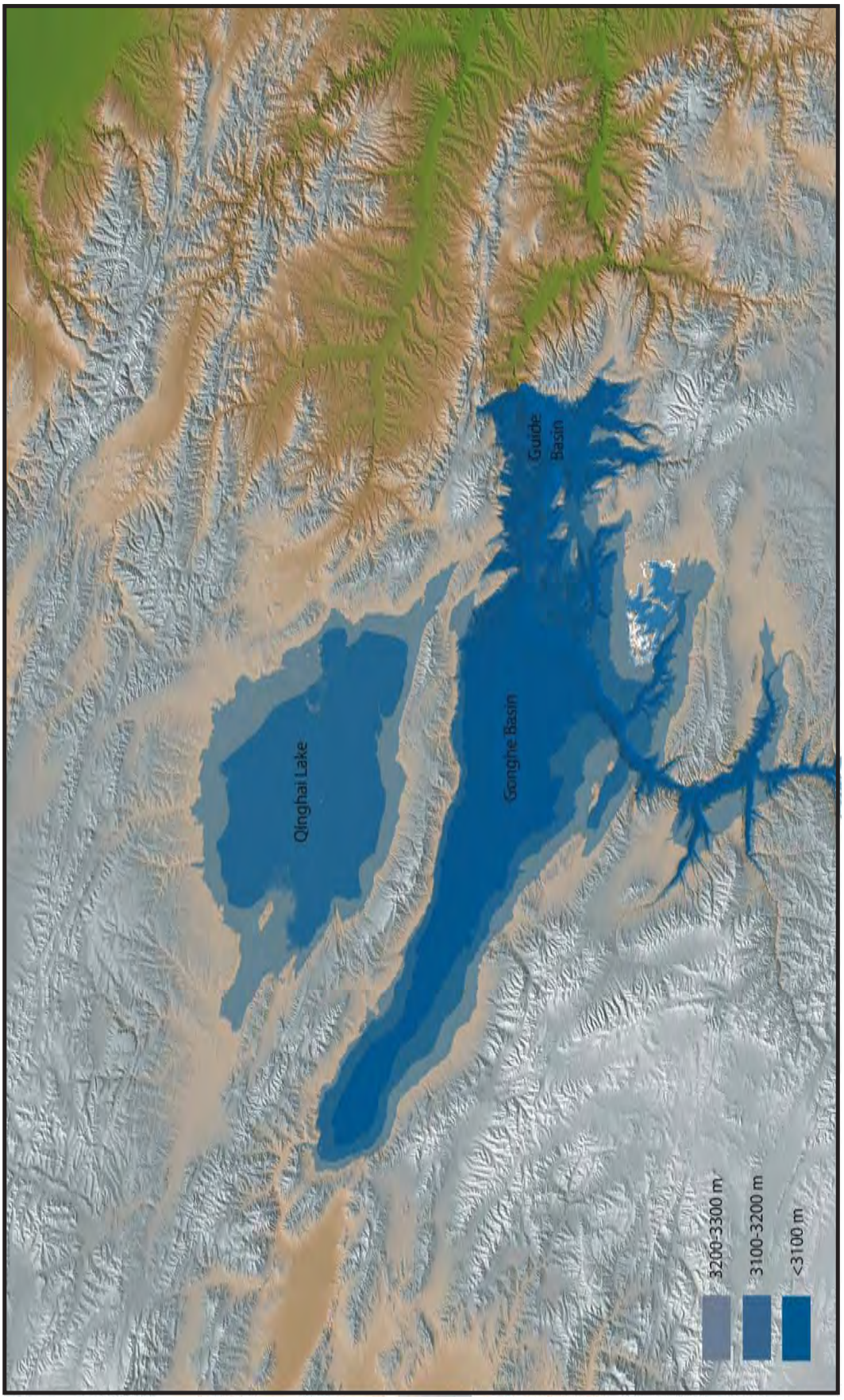
Qinghai Lake
Gonghe Basin
Guide Basin
3200-3300 m
3100-3200 m
<3100 m

Figure 17

Sample name	Sample description	Latitude (°N)	Longitude (°E)	Elevation (m a.s.l.)	Depth (cm)	Sample thickness (cm)	10Be concentration (atomes/g)	err	26Al concentration (atomes/g)	err	[26Al]/[10Be] ratio	err
Terrace T5												
Qi4-30	quartz cobble	36.17584	100.52143	2920	0	3	2.98E+06	8.44E+04	na	na	na	na
Qi4-30-2§							3.12E+06	8.87E+04	na	na	na	na
Qi4-33	quartz cobble	36.17567	100.52181	2920	0	4	2.98E+06	8.57E+04	na	na	na	na
Qi4-34	quartz cobble	36.17520	100.52123	2920	0	8	3.26E+06	9.37E+04	na	na	na	na
Qi4-36	quartz cobble	36.17532	100.521	2918	0	5.5	3.27E+06	9.27E+04	na	na	na	na
Qi4-36-2§							3.34E+06	9.77E+04	na	na	na	na
Qi4-38	quartz cobble	36.17555	100.52113	2920	0	6	3.05E+06	9.43E+04	na	na	na	na
Qi4-39	quartz cobble	36.17566	100.52179	2919	0	8	3.74E+06	1.02E+05	na	na	na	na
Qi4-40	quartz cobble	36.17595	100.52154	2920	0	5	2.84E+06	8.52E+04	na	na	na	na
Terrace T7												
Qi4-29-1*	quartz cobble	35.70043	100.29636	3196	200	5	9.55E+05	2.56E+04	4.64E+06	5.33E+05	4.86	0.57
Qi4-29-27a ⊏	8 amalgamated pebbles	35.70043	100.29636	3194	200-220	2	1.53E+06	4.39E+04	na	na	na	na
Qi4-29-27b ⊏	13 amalgamated pebbles	35.70043	100.29636	3194	200-220	2	1.32E+06	4.04E+04	na	na	na	na
Qi4-29-27c ⊏	32 amalgamated pebbles	35.70043	100.29636	3194	200-220	1.5	1.47E+06	6.43E+04	8.88E+06	4.31E+05	6.03	0.39
Qi4-29-27d ⊏	55 amalgamated pebbles	35.70043	100.29636	3194	200-220	1	1.54E+06	5.53E+04	9.11E+06	3.94E+05	5.91	0.33
							Weighted mean : 1.4615E+06 ±0.1031E+06					
Qi4-29-19*	quartz cobble	35.70043	100.29636	3194	230	4	1.07E+06	2.85E+04	6.33E+06	2.13E+05	5.89	0.25
Qi4-29-9	quartz cobble	35.70043	100.29636	3194	240	4.5	2.13E+06	7.31E+04	8.77E+06	3.80E+05	4.12	0.23
Qi4-29-13	quartz cobble	35.70043	100.29636	3194	260	5.5	7.66E+05	2.83E+04	na	na	na	na
Qi4-29-11	quartz cobble	35.70043	100.29636	3194	320	6	3.97E+05	1.61E+04	2.43E+06	1.11E+05	6.12	0.37
Qi4-29-11-2§							4.00E+05	1.59E+04	na	na	na	na
Qi4-29-14	sand lens	35.70043	100.29636	3194	370	2	7.85E+05	2.74E+04	3.79E+06	1.51E+05	4.83	0.25
Qi4-29-15	sand lens	35.70043	100.29636	3194	390	2	5.05E+05	1.75E+04	2.46E+06	9.65E+04	4.87	0.26
Qi4-29-16	quartz cobble	35.70043	100.29636	3194	400	6	6.18E+05	2.45E+04	3.66E+06	1.62E+05	5.93	0.35
Qi4-29-21	quartz cobble	35.70043	100.29636	3194	615	5	2.35E+05	9.48E+03	1.34E+06	6.88E+04	5.69	0.37
Qi4-29-22	quartz cobble	35.70043	100.29636	3194	675	9	1.90E+06	6.54E+04	9.67E+06	4.12E+05	5.09	0.28
Qi4-29-23	sand lens	35.70043	100.29636	3194	750	2	4.45E+05	1.87E+04	2.25E+06	2.03E+05	5.06	0.50
Qi4-29-24	quartz cobble	35.70043	100.29636	3194	480	6	5.38E+05	2.04E+04	3.26E+06	1.35E+05	6.06	0.34
Terrace WRB												
Qi4-47	granitic bedrock	36.12209	100.93520	2680	0	4	1.28E+06	3.72E+04	na	na	na	na
Qi4-47-2§							1.40E+06	5.74E+04	na	na	na	na
Qi4-48	granitic bedrock	36.12221	100.93571	2680	0	3.5	1.18E+06	3.44E+04	na	na	na	na
Qi4-49	granitic bedrock	36.12184	100.93532	2683	0	3.5	1.90E+06	7.73E+04	na	na	na	na
Qi4-50	cobble	36.12196	100.93521	2680	0	8	1.91E+06	5.46E+04	na	na	na	na
Qi4-51	cobble	36.12203	100.93511	2680	0	8	1.89E+06	5.43E+04	na	na	na	na
Qi4-52	cobble	36.12212	100.93505	2682	0	8	1.85E+06	6.26E+04	na	na	na	na
Qi4-53	cobble	36.12212	100.93505	2681	0	4	1.90E+06	6.11E+04	na	na	na	na
Qi4-54	cobble	36.12214	100.93503	2681	0	4	1.89E+06	6.28E+04	1.17E+07	5.83E+05	6.16	0.37
Terrace WLB												
Qi4-59	quartz vein in bedrock	36.13491	100.95922	2925	0	8	5.61E+05	1.91E+04	na	na	na	na
Qi4-60	granitic bedrock	36.13455	100.95926	2934	0	3.5	1.82E+06	6.16E+04	na	na	na	na
Qi4-61	cobble	36.13449	100.96021	2938	0	4	2.64E+06	9.86E+04	na	na	na	na
Qi4-61-2§							2.58E+06	8.39E+04	na	na	na	na
Qi4-62	granitic bedrock	36.13405	100.96105	2940	0	3	2.49E+06	7.56E+04	1.30E+07	5.30E+05	5.23	0.27

Yellow river sand											
Qi4-43A	river sand	36.12972	100.9967	2367	0		3.09E+05	1.24E+04	1.63E+06	7.63E+04	5.28	0.32

na: not analized
*: AMS measurements at CAMS at Lawrence Livermore National Laboratory
☐: see details of sample characteristics in Figure 9.
§: duplicate of the same sample after quartz leaching.

Table 1.

Table 2. Depth profile model parameters (see Figure 10).

Model	Inheritance (at/g quartz)	Exposure of C1 (ka)	Erosion rate (cm/yr)	Exposure of C2 (ka)	Erosion rate (cm/yr)	Duration of loess deposit (ka)	Exposure loess (ka)	Erosion rate (cm/yr)	Total duration of exposure (ka)
1	235000	15	0	45	0.005	1	150	0.0001	210
2	445000	15	0	20	0	1	80	0	115
3	235000	15	0	50	0		400	0.01	465
models of figure 10c	235000	15	0	15	0	50	10	0	90
	235000	15	0	15	0	25	70	0	125
	235000	15	0	15	0	10	120	0	160
	235000	15	0	15	0	1	150	0	181

Table 2.